Quaternion Invariant Extended Kalman Filtering for Spacecraft Attitude Estimation

Article *in* Journal of Guidance Control and Dynamics · December 2017

DOI: 10.2514/1.G003177

CITATIONS
4

READS
254

2 authors:

Haichao Gui
Beihang University (BUAA)
44 PUBLICATIONS **305** CITATIONS
SEE PROFILE

Anton H. J. de Ruiter
Ryerson University
82 PUBLICATIONS **477** CITATIONS
SEE PROFILE

Quaternion Invariant Extended Kalman Filtering for Spacecraft Attitude Estimation

Haichao Gui[1]
Beihang University, Beijing, P.R. China, 100191

Anton H. J. de Ruiter[2]
Ryerson University, Toronto, Ontario, Canada, M5B 2K3

The spacecraft attitude estimation is addressed in the framework of invariant Kalman filtering, which rests on invariance of the system dynamics and output map with respect to appropriate coordinate transformations. The available measurements are assumed to be the angular velocity from three-axis gyroscopes and vector measurements from attitude sensors. Two continuous-discrete quaternion filters are developed from output-state errors defined in the inertial frame and the spacecraft body frame respectively. The former is termed the right-invariant extended Kalman filter (RIEKF) and the latter left-invariant extended Kalman filter (LIEKF). These two filters both respect the norm constraint of the attitude quaternion but stem from different invariance properties of the system dynamics. It is shown that the LIEKF bears much resemblance to, and thus can be viewed as a minor variant of the conventional quaternion multiplicative extended Kalman filter (MEKF). The RIEKF possesses less dependence on the estimated trajectory and, as a result, better robustness than the LIEKF and MEKF. Extensive Monte Carlo simulations of spacecraft attitude determination implementations demonstrate the advantageous performance of the RIEKF, compared to the LIEKF, MEKF, and some of their improved variants.

---

[1] School of Astronautics, 37 Xueyuan Road, Beijing, 100191, P.R. China
[2] Department of Aerospace Engineering, 350 Victoria Street, Toronto, ON, M5B 2K3, Canada

Nomenclature

$\boldsymbol{A}(\boldsymbol{q})$ = 3-by-3 rotation matrix as a function of the attitude quaternion $\boldsymbol{q}$

$\boldsymbol{I}_n$ = $n \times n$ identity matrix

$\boldsymbol{P}$ = covariance matrix of the state estimation error

$\boldsymbol{q}$ = the spacecraft attitude quaternion

$\boldsymbol{r}^i$ = the ith known vector expressed in the inertial frame

$\mathcal{F}_B$ = spacecraft body-fixed frame

$\mathcal{F}_I$ = inertial frame

$\mathbb{H}$ = the set of quaternions

$\mathbb{S}^3$ = the set of unit quaternions

$\boldsymbol{\omega}$ = spacecraft angular velocity vector expressed in $\mathcal{F}_B$, rad/s

$\bar{\boldsymbol{\omega}}$ = measurement of the spacecraft angular velocity vector, rad/s

$\boldsymbol{\beta}$ = gyro bias, rad/s

$\boldsymbol{\eta}_v$, $\boldsymbol{\eta}_u$ = gyro noise processes

$\boldsymbol{v}^i$ = white Gaussian noise process associated with the i-th vector measurement

$\boldsymbol{g}$ = group element and serves as the state variable $\boldsymbol{x}$ with $\boldsymbol{g} = (\boldsymbol{q}, \boldsymbol{\beta})$

$\boldsymbol{u}$ = the system input variable defined as $\boldsymbol{u} = (\bar{\boldsymbol{\omega}}, \boldsymbol{r}^1, \cdots, \boldsymbol{r}^n)$

$\|\cdot\|$ = Euclidean norm of a vector

Superscript

T = transpose of a vector or matrix

$\hat{}$ = estimate of a state variable

$\tilde{}$ = estimation error of a state variable

$-$ = a priori estimate of a variable

$+$ = a posteriori estimate of a variable

Subscript

k = the value of a vector or matrix at time t_k

I. Introduction

The knowledge of the spacecraft attitude, which forms a 3-dimensional compact manifold, is essential for its on-orbit operation. Since the spacecraft attitude cannot be directly measured, it is usually derived from body-frame observations of reference vectors, usually complemented with angular velocity measurements from gyroscopes for improved accuracy. Various attitude estimation algorithms have been proposed, including algebraic approaches using merely vector measurements such as TRIAD [1, 2], QUEST [3, 4] and ESOQ [5], and dynamical approaches that combine sensor measurements with spacecraft attitude equations such as extended Kalman filters (EKF) [6–9] and deterministic observers [10–12]. A comprehensive survey of spacecraft attitude estimation algorithms can be found in [13].

Among the existing methods, the multiplicative EKF (MEKF) in terms of quaternions has achieved broad applications because it is nonsingular and involves fewer parameters than the SO(3) formulation [14]. The fundamental idea is to estimate the attitude error with three-parameter formulations, such as the rotation vector, Euler angles, Rodrigues parameters, modified Rodrigues parameters, etc, while using a unit quaternion to represent the estimated attitude. This idea does not entail, but some implementations of the MEKF still require, a brute-force normalization step in the filtering algorithm [15]. In order to accommodate this issue, continuous-time and discrete-time constrained Kalman filters (CKF) preserving the norm constraint were developed [16, 17]. It was shown that brute-force normalization after the measurement update, as adopted in the quaternion MEKF, is in fact optimal [16].

The EKF methods such as the MEKF work by linearizing nonlinear systems about the estimated trajectory and then applying the Kalman filter to the linearized system. Hence, their performance largely relies on validity of the small error assumption and is sensitive to the initial state guess. With poor initial estimation, the EKF can exhibit degraded performance or even diverge. To overcome this drawback, improvements within the EKF framework were presented in [18], where an extended QUEST algorithm was proposed, and in [19], where a q-method EKF was developed. These methods attempted to incorporate the algebraic attitude determination algorithm into the classical EKF. Reynolds [20] introduced a covariance resetting after measurement update with proven convergence

for attitude estimation without gyroscope bias. This idea has recently been extended in [21] to include other states for estimation. In order to achieve high-order approximations to the nonlinearity intrinsic in attitude equations, unscented filters [22] and particle filters [23] are alternative choices. They can provide more robustness and better estimation accuracy but expend more computational resources than the EKF methods.

Recently, the invariant extended Kalman filtering (IEKF) has emerged as an appealing improvement to the conventional EKF with comparable computational efficiency [24, 25]. It is a consequence of the combination between the invariant observer theory [26, 27] and EKF, and applies to dynamical systems possessing invariance properties. Here, invariance refers to the case that the system dynamics and the corresponding output map stay unchanged with respect to proper coordinate transformations on the state, input, and output variables. The IEKF builds on invariant output errors and estimation errors for filter development. Furthermore, it performs the measurement update in a nonlinear manner that preserves the geometry of the state manifold, rather than in a linear form as the EKF. When the invariant output error and state estimation error are appropriately constructed, the dependence of the resultant IEKF on the estimated trajectory can be reduced or even eliminated (neglecting the case when external forces or torques rely on estimated states), yielding increased robustness in the estimation algorithm. Continuous-time IEKFs were designed for inertial navigation of unmanned aerial vehicles in [25, 28], aided with velocity measurements and global positioning system respectively. Discrete-time IEKF posed on SO(3) for attitude estimation was developed in [29] assuming the absence of gyro biases. In reality, the rate measurements of gyroscopes drift over time and its effect needs to be compensated for long-period, accurate attitude determination.

This paper studies the spacecraft attitude determination issue using angular velocity measurements from rate gyros and vector measurements from attitude sensors such as sun sensors, magnetometers, star trackers, etc. Two quaternion IEKFs involving continuous dynamics and discrete measurements (which are briefed as "continuous-discrete") are developed in sequence through the invariant Kalman filtering theory, namely, the right-invariant extended Kalman filter (RIEKF) and the left-invariant extended Kalman filter (LIEKF). Both filters preserve the unit-norm constraint

of attitude quaternions by generating corrections with the quaternion exponential map but their individual structures differ greatly. They root in two different types of invariance properties of the system equations. More precisely, the RIEKF features an invariant output error and a state estimation error evaluated in the inertial frame. In contrast, the LIEKF features an invariant output error and a state estimation error evaluated in the spacecraft body frame, which are exactly the same as those of the classical quaternion MEKF. It is revealed that the MEKF is, in fact, a variant of the LIEKF with corrections approximated in the first order. Compared to the LIEKF and MEKF, the RIEKF possesses less dependence on the estimated trajectory, e.g., the sensitivity matrix and the attitude estimation error equation are both independent of the estimated attitude and bias as well as the angular velocity measurement. Extensive Monte Carlo simulations of a spacecraft attitude determination example indicate that the RIEKF is more robust to initial conditions and provides better prediction on the estimation uncertainty than the LIEKF, MEKF, CKF [16], and the variants of the MEKF and LIEKF improved with the covariance mapping derived in [21].

The remainder of this paper is organized as follows: Section II presents some basics on quaternion algebra, system equations, and invariant dynamical systems. The RIEKF and LIEKF are developed successively in Section III and IV based on two different types of invariant output-state errors. Section V discusses the differences and similarities between the RIEKF, LIEKF, and MEKF. Numerical simulations are given in Section VI to demonstrate the effectiveness of the proposed filters and conclusions are drawn in Section VII.

II. Preliminaries and System Models

A. Quaternions

Denote by $\mathbb{H}$ the set of quaternions, which is actually isomorphic to $\mathbb{R}^4$. A quaternion can be represented as $\boldsymbol{q} = [q_0, \boldsymbol{q}_v^T]^T \in \mathbb{H}$, where $q_0 \in \mathbb{R}$ and $\boldsymbol{q}_v = [q_1, q_2, q_3]^T \in \mathbb{R}^3$ are called the scalar and vector parts of $\boldsymbol{q}$, respectively. The conjugate of $\boldsymbol{q}$ is also an element in $\mathbb{H}$ and is given by $\boldsymbol{q}^* = [q_0, -\boldsymbol{q}_v^T]^T$. The quaternion product between $\boldsymbol{q}$ and any $\boldsymbol{p} = [p_0, \boldsymbol{p}_v^T]^T \in \mathbb{H}$ is defined as

$$\boldsymbol{q} \otimes \boldsymbol{p} = \begin{bmatrix} q_0 p_0 - \boldsymbol{q}_v^T \boldsymbol{p}_v \\ q_0 \boldsymbol{p}_v + p_0 \boldsymbol{q}_v + \boldsymbol{q}_v \times \boldsymbol{p}_v \end{bmatrix}$$

The above binary operation is both associative and distributive but is not commutative. In addition, it is direct to verify that $(\boldsymbol{q} \otimes \boldsymbol{p})^* = \boldsymbol{p}^* \otimes \boldsymbol{q}^*$. Note that the vectors in $\mathbb{R}^3$ can be viewed as quaternions with zero scalar parts and therefore the quaternion product and conjugation operations can also be applied to them.

Unit quaternions are quaternions with unit length and comprise of the unit sphere in $\mathbb{R}^4$, i.e, the three dimensional unit sphere. Letting $\mathbf{1} = [1, 0, 0, 0]^T$ be the identity in $\mathbb{H}$, the set of unit quaternions is then defined by $\mathbb{S}^3 = \{\boldsymbol{q} \in \mathbb{H} : \boldsymbol{q} \otimes \boldsymbol{q}^* = \boldsymbol{q}^* \otimes \boldsymbol{q} = \mathbf{1}\}$. Clearly, the inverse of a unit quaternion is identical to its conjugate. Unit quaternions provide a global non-singular representation of the rotations in $\mathbb{R}^3$, whose set is denoted by SO(3). Given a rotation about the unit axis $\boldsymbol{\eta} \in \mathbb{R}^3$ ($\|\boldsymbol{\eta}\| = 1$) at an angle $\phi \in \mathbb{R}$, the corresponding unit quaternion is given by

$$\boldsymbol{q} = \begin{bmatrix} \cos\left(\frac{\phi}{2}\right) \\ \boldsymbol{\eta} \sin\left(\frac{\phi}{2}\right) \end{bmatrix} \tag{1}$$

which gives rise to a rotation matrix

$$\boldsymbol{A}(\boldsymbol{q}) = (q_0^2 - \boldsymbol{q}_v^T \boldsymbol{q}_v)\boldsymbol{I}_3 + 2\boldsymbol{q}_v \boldsymbol{q}_v^T - 2q_0 \boldsymbol{q}_v^\times$$

where $\boldsymbol{I}_n$ is the $n \times n$ identity matrix and

$$\boldsymbol{q}_v^\times = \begin{bmatrix} 0 & -q_3 & q_2 \\ q_3 & 0 & -q_1 \\ -q_2 & q_1 & 0 \end{bmatrix}$$

Since $\boldsymbol{A}(\boldsymbol{q}) = \boldsymbol{A}(-\boldsymbol{q})$, unit quaternions form a double covering of SO(3). For all $\boldsymbol{x} \in \mathbb{R}^3$, $\boldsymbol{q}$ and $\boldsymbol{A}(\boldsymbol{q})$ satisfy the following relations

$$\boldsymbol{A}(\boldsymbol{q})\boldsymbol{x} = \boldsymbol{q}^* \otimes \boldsymbol{x} \otimes \boldsymbol{q} \tag{2}$$

$$\boldsymbol{A}^T(\boldsymbol{q})\boldsymbol{x} = \boldsymbol{A}(\boldsymbol{q}^*)\boldsymbol{x} = \boldsymbol{q} \otimes \boldsymbol{x} \otimes \boldsymbol{q}^* \tag{3}$$

The quaternion exponential map from $\mathbb{R}^3$ to $\mathbb{S}^3$ has a simple closed form [30]:

$$\exp_q(\boldsymbol{x}) = \sum_{n=0}^{\infty} \frac{1}{n!} \underbrace{(\boldsymbol{x} \otimes \cdots \otimes \boldsymbol{x})}_{n \text{ times}} = \begin{bmatrix} \cos(\|\boldsymbol{x}\|) \\ \\ \frac{\boldsymbol{x}}{\|\boldsymbol{x}\|} \sin(\|\boldsymbol{x}\|) \end{bmatrix} \tag{4}$$

Given the principal rotation vector $\phi\boldsymbol{\eta} \in \mathbb{R}^3$, it is readily seen that $\exp_q(\phi\boldsymbol{\eta}/2)$ reduces to the unit quaternion defined in Eq. (1).

B. System Model

Consider a rigid spacecraft and denote by $\mathcal{F}_B$ its body-fixed frame. Let $\boldsymbol{q}(t) \in \mathbb{S}^3$ represent the attitude of the spacecraft with respect to the inertial frame $\mathcal{F}_I$. The attitude kinematics in terms of the unit quaternion are written as

$$\dot{\boldsymbol{q}}(t) = \frac{1}{2}\boldsymbol{q}(t) \otimes \boldsymbol{\omega}(t) \tag{5}$$

where $\boldsymbol{\omega}(t) \in \mathbb{R}^3$ is the spacecraft angular velocity relative to $\mathcal{F}_I$ expressed in $\mathcal{F}_B$.

The spacecraft angular velocity is commonly measured by the onboard rate gyroscopes. The typical measurement model is given by [31]

$$\boldsymbol{\omega}(t) = \bar{\boldsymbol{\omega}}(t) - \boldsymbol{\beta}(t) - \boldsymbol{\eta}_v(t) \tag{6}$$

$$\dot{\boldsymbol{\beta}}(t) = \boldsymbol{\eta}_u(t) \tag{7}$$

where $\bar{\boldsymbol{\omega}}(t)$ is the output signal from the rate gyros and $\boldsymbol{\beta}(t)$ represents the gyro bias vector; $\boldsymbol{\eta}_v(t)$ and $\boldsymbol{\eta}_u(t)$ are zero-mean white noise processes with autocovariances

$$\begin{aligned} E\{\boldsymbol{\eta}_v(t)\boldsymbol{\eta}_v^T(\tau)\} &= \sigma_v^2\delta(t-\tau)\boldsymbol{I}_3 \\ E\{\boldsymbol{\eta}_u(t)\boldsymbol{\eta}_u^T(\tau)\} &= \sigma_u^2\delta(t-\tau)\boldsymbol{I}_3 \end{aligned}$$

where $\delta(\cdot)$ is the Dirac-delta function and $\boldsymbol{\eta}_v(t)$ and $\boldsymbol{\eta}_u(t)$ are independent. In addition, attitude sensors, such as sun sensors, magnetometers and star trackers, are utilized to provide vector measurements and the corresponding measurement model is given by

$$\boldsymbol{y}^i(t) = \boldsymbol{q}^*(t) \otimes \boldsymbol{r}^i(t) \otimes \boldsymbol{q}(t) + \boldsymbol{v}^i(t), \quad i = 1, \cdots, n$$

where $\boldsymbol{r}^i(t) \in \mathbb{R}^3$, $i = 1, \cdots, n$, are known vectors expressed in $\mathcal{F}_I$ and $\boldsymbol{y}^i(t)$, $i = 1, \cdots, n$, are the corresponding measurements in $\mathcal{F}_B$; $\boldsymbol{v}^i(t) \in \mathbb{R}^3$, $i = 1, \cdots, n$, denote the sensor noise modeled as zero-mean white Gaussian processes. The autocovariance of the vector measurement noise at times t_k and t_l is given by

$$E\{\boldsymbol{v}^i(t_k)(\boldsymbol{v}^j(t_l))^T\} = \delta_{kl}\boldsymbol{R}^{ij}(t_k)$$

where $\delta_{kl} = 1$ if $k = l$, and $\delta_{kl} = 0$ otherwise; $\boldsymbol{R}^{ij}(t_k) \in \mathbb{R}^{3\times 3}$ is a positive-definite symmetric matrix. At least two non-collinear vector measurements are assumed to be available in order to guarantee the observability of the system. In the following, the time argument of functions and variables are omitted unless clarity is required.

Letting $\boldsymbol{y} = [(\boldsymbol{y}^1)^T, \cdots, (\boldsymbol{y}^n)^T] \in \mathbb{R}^{3n}$ and $\boldsymbol{V} = [(\boldsymbol{v}^1)^T, \cdots, (\boldsymbol{v}^n)^T] \in \mathbb{R}^{3n}$, the above vector measurements can also be written in the aggregated form

$$\boldsymbol{y} = \boldsymbol{h}(\boldsymbol{q}, \boldsymbol{\beta}, \boldsymbol{u}) + \boldsymbol{V}, \quad \boldsymbol{h}(\boldsymbol{q}, \boldsymbol{\beta}, \boldsymbol{u}) = \begin{bmatrix} \boldsymbol{q}^* \otimes \boldsymbol{r}^1 \otimes \boldsymbol{q} \\ \vdots \\ \boldsymbol{q}^* \otimes \boldsymbol{r}^n \otimes \boldsymbol{q} \end{bmatrix} \tag{8}$$

where $(\boldsymbol{q}, \boldsymbol{\beta})$ is the state and and $\boldsymbol{u} = (\bar{\boldsymbol{\omega}}, \boldsymbol{r}^1, \cdots, \boldsymbol{r}^n) \in \mathbb{R}^{3(n+1)}$ is the input of the system given in Eqs. (5)-(7). In addition, define the following matrix

$$\boldsymbol{R}_k = \begin{bmatrix} \boldsymbol{R}^{11}(t_k) & \boldsymbol{R}^{12}(t_k) & \cdots & \boldsymbol{R}^{1n}(t_k) \\ \vdots & \vdots & \vdots & \vdots \\ \boldsymbol{R}^{n1}(t_k) & \boldsymbol{R}^{n2}(t_k) & \cdots & \boldsymbol{R}^{nn}(t_k) \end{bmatrix}$$

which represents the autocovariance of $\boldsymbol{V}$ at time t_k.

Substituting Eq. (6) into Eq. (5) and omitting the noisy terms in Eqs. (6)-(8), one can obtain the following noise-free system model

$$\begin{cases} \dot{\boldsymbol{q}} &= \frac{1}{2}\boldsymbol{q} \otimes (\bar{\boldsymbol{\omega}} - \boldsymbol{\beta}) \\ \dot{\boldsymbol{\beta}} &= 0 \\ \boldsymbol{y} &= \boldsymbol{h}(\boldsymbol{q}, \boldsymbol{\beta}, \boldsymbol{u}) \end{cases} \tag{9}$$

C. Invariance Properties

Consider the smooth system

$$\begin{cases} \dot{\boldsymbol{x}} &= \boldsymbol{f}(\boldsymbol{x}, \boldsymbol{u}) \\ \boldsymbol{y} &= \boldsymbol{h}(\boldsymbol{x}, \boldsymbol{u}) \end{cases} \quad \boldsymbol{x} \in X,\, \boldsymbol{u} \in U,\, \boldsymbol{y} \in Y \tag{10}$$

where $X \subset \mathbb{R}^n$, $U \subset \mathbb{R}^m$, and $Y \subset \mathbb{R}^p$ are the state space, input space, and output space of proper dimensions, respectively. Let G be a Lie group with the identity element $\boldsymbol{e}$. Given $\boldsymbol{g} \in G$, a smooth map $\varphi_g : G \times X \to X$ is called a Lie group action on X if it satisfies $\phi_e(\boldsymbol{x}) = \boldsymbol{x}$ and $\varphi_{g_r}(\varphi_g(\boldsymbol{x})) = \varphi_{g_r g}(\boldsymbol{x})$ for all $\boldsymbol{g}_r \in G$, $\boldsymbol{x} \in X$. Similarly, denote by ψ_g and ρ_g the group actions on U and Y respectively. The following definitions, first introduced in [27], are used to describe symmetries of systems of the form as Eq. (10).

Definition 1: The system (10) is G-invariant if $\mathrm{d}\varphi_g(\boldsymbol{x})/\mathrm{d}t = \boldsymbol{f}(\varphi_g(\boldsymbol{x}), \psi_g(\boldsymbol{u}))$ for all $\boldsymbol{g}, \boldsymbol{x}, \boldsymbol{u}$.

Definition 2: The output of system (10) is G-equivariant if there exists a group action ρ_g on Y such that $\boldsymbol{h}(\varphi_g(\boldsymbol{x}), \psi_g(\boldsymbol{u})) = \rho_g(\boldsymbol{h}(\boldsymbol{x}, \boldsymbol{u}))$ for all $\boldsymbol{g}, \boldsymbol{x}, \boldsymbol{u}$.

In fact, the preceding group actions φ_g, ψ_g, and ρ_g can be intuitively viewed as some coordinate transformations, with respect to which the invariant quantities in this paper are defined. Denote by $\hat{\boldsymbol{x}} \in X$ an estimate of the state $\boldsymbol{x}$. The output error is a smooth map $(\hat{\boldsymbol{x}}, \boldsymbol{u}, \boldsymbol{y}) \longmapsto \mathcal{E}(\hat{\boldsymbol{x}}, \boldsymbol{u}, \boldsymbol{y}) \in \mathbb{R}^p$ that is invertible for all $\hat{\boldsymbol{x}}, \boldsymbol{u}$ and satisfies $\mathcal{E}(\hat{\boldsymbol{x}}, \boldsymbol{u}, \boldsymbol{y}) = 0 \Leftrightarrow \boldsymbol{x} = \hat{\boldsymbol{x}}$. Furthermore, it is called an invariant output error if $\mathcal{E}(\varphi_g(\hat{\boldsymbol{x}}), \psi_g(\boldsymbol{u}), \rho_g(\boldsymbol{y})) = \mathcal{E}(\hat{\boldsymbol{x}}, \boldsymbol{u}, \boldsymbol{y})$. The smooth map $(\boldsymbol{x}, \hat{\boldsymbol{x}}) \longmapsto \mathcal{S}(\boldsymbol{x}, \hat{\boldsymbol{x}}) \in \mathbb{R}^n$ is called an invariant estimation error if $\mathcal{S}(\boldsymbol{x}, \hat{\boldsymbol{x}}) = 0 \Leftrightarrow \boldsymbol{x} = \hat{\boldsymbol{x}}$ and $\mathcal{S}(\varphi_g(\boldsymbol{x}), \varphi_g(\hat{\boldsymbol{x}})) = \mathcal{S}(\boldsymbol{x}, \hat{\boldsymbol{x}})$ for all $\boldsymbol{g}, \boldsymbol{x}, \hat{\boldsymbol{x}}$. Assume that system (10) is G-invariant with G-equivariant output. If the state space X is identical to the Lie group G, then an invariant output error is given by $\mathcal{E}(\hat{\boldsymbol{x}}, \boldsymbol{u}, \boldsymbol{y}) = \rho_{\hat{\boldsymbol{x}}^{-1}}(\boldsymbol{h}(\hat{\boldsymbol{x}}, \boldsymbol{u})) - \rho_{\hat{\boldsymbol{x}}^{-1}}(\boldsymbol{y})$ (or $\rho_{\hat{\boldsymbol{x}}^{-1}}(\boldsymbol{y}) - \rho_{\hat{\boldsymbol{x}}^{-1}}(\boldsymbol{h}(\hat{\boldsymbol{x}}, \boldsymbol{u}))$) [25].

III. Right Invariant Extended Kalman Filter Design

A. Invariant Output Errors and Estimation Errors

Consider the attitude system (9), which bears the same form as Eq. (10) with $(\boldsymbol{q}, \boldsymbol{\beta}) \in \mathbb{S}^3 \times \mathbb{R}^3$, $\boldsymbol{u} = (\bar{\boldsymbol{\omega}}, \boldsymbol{r}^1, \cdots, \boldsymbol{r}^n) \in \mathbb{R}^{3(n+1)}$, and $\boldsymbol{h}(\boldsymbol{q}, \boldsymbol{\beta}, \boldsymbol{u}) \in \mathbb{R}^{3n}$ being the state, input and output. It has been noticed in [26] that $\mathbb{S}^3 \times \mathbb{R}^3$ forms a Lie group under the following group composition:

$$\begin{pmatrix} \boldsymbol{q}_r \\ \boldsymbol{\beta}_r \end{pmatrix} \circ \begin{pmatrix} \boldsymbol{q} \\ \boldsymbol{\beta} \end{pmatrix} = \begin{pmatrix} \boldsymbol{q} \otimes \boldsymbol{q}_r \\ \boldsymbol{q}_r^* \otimes \boldsymbol{\beta} \otimes \boldsymbol{q}_r + \boldsymbol{\beta}_r \end{pmatrix} \tag{11}$$

where $(\boldsymbol{q}_r, \boldsymbol{\beta}_r), (\boldsymbol{q}, \boldsymbol{\beta}) \in \mathbb{S}^3 \times \mathbb{R}^3$.

Hereafter, denote by $G = \mathbb{S}^3 \times \mathbb{R}^3$, $\boldsymbol{g} = (\boldsymbol{q}, \boldsymbol{\beta}) \in G$ and $\boldsymbol{h}(\boldsymbol{g}, \boldsymbol{u}) = \boldsymbol{h}(\boldsymbol{q}, \boldsymbol{\beta}, \boldsymbol{u})$. The identity element on G is $(\mathbf{1}, 0) \in G$ since $\boldsymbol{g} \circ (\mathbf{1}, 0) = (\mathbf{1}, 0) \circ \boldsymbol{g} = \boldsymbol{g}$ for all $\boldsymbol{g} \in G$. In addition, the inverse of $\boldsymbol{g}$ is found to be

$$\boldsymbol{g}^{-1} = \begin{pmatrix} \boldsymbol{q}^* \\ -\boldsymbol{q} \otimes \boldsymbol{\beta} \otimes \boldsymbol{q}^* \end{pmatrix} \tag{12}$$

Given $\boldsymbol{g}_r = (\boldsymbol{q}_r, \boldsymbol{\beta}_r) \in G$, define

$$\begin{aligned} \varphi_{g_r}(\boldsymbol{g}) &= \boldsymbol{g}_r \circ \boldsymbol{g} \\ \psi_{g_r}(\boldsymbol{u}) &= (\boldsymbol{q}_r^* \otimes (\bar{\boldsymbol{\omega}} + \boldsymbol{\beta}_r) \otimes \boldsymbol{q}_r, \boldsymbol{r}^1, \cdots, \boldsymbol{r}^n) \end{aligned}$$

as the group actions of G on the state space and input space respectively. It can then be readily verified that system (9) satisfies Definition 1 and is hence G-invariant. In addition, one can also define a group action on $\mathbb{R}^{3n}$ as

$$\rho_{g_r} \boldsymbol{h}(\boldsymbol{g}, \boldsymbol{u}) = \boldsymbol{h}(\varphi_{g_r}(\boldsymbol{g}), \psi_{g_r}(\boldsymbol{u})) = \begin{bmatrix} \boldsymbol{q}_r^* \otimes \boldsymbol{b}^1 \otimes \boldsymbol{q}_r \\ \vdots \\ \boldsymbol{q}_r^* \otimes \boldsymbol{b}^n \otimes \boldsymbol{q}_r \end{bmatrix}$$

such that the output of the system is G-equivariant.

Denote by $\hat{\boldsymbol{g}} = (\hat{\boldsymbol{q}}, \hat{\boldsymbol{\beta}}) \in G$ a state estimate. An invariant output error is then derived as

$$\mathcal{E}(\hat{\boldsymbol{g}}, \boldsymbol{u}, \boldsymbol{y}) = \rho_{\hat{g}^{-1}}(\boldsymbol{h}(\hat{\boldsymbol{g}}, \boldsymbol{u})) - \rho_{\hat{g}^{-1}}(\boldsymbol{y}) = \begin{bmatrix} \boldsymbol{r}^1 \\ \vdots \\ \boldsymbol{r}^n \end{bmatrix} - \begin{bmatrix} \hat{\boldsymbol{q}} \otimes \boldsymbol{b}^1 \otimes \hat{\boldsymbol{q}}^* \\ \vdots \\ \hat{\boldsymbol{q}} \otimes \boldsymbol{b}^n \otimes \hat{\boldsymbol{q}}^* \end{bmatrix} \tag{13}$$

Additionally, define the following estimation errors:

$$\tilde{\boldsymbol{g}}(\boldsymbol{g}, \hat{\boldsymbol{g}}) = \begin{pmatrix} \tilde{\boldsymbol{q}} \\ \tilde{\boldsymbol{\beta}} \end{pmatrix} = \boldsymbol{g}^{-1} \circ \hat{\boldsymbol{g}} = \begin{pmatrix} \hat{\boldsymbol{q}} \otimes \boldsymbol{q}^* \\ \boldsymbol{q} \otimes (\hat{\boldsymbol{\beta}} - \boldsymbol{\beta}) \otimes \boldsymbol{q}^* \end{pmatrix} \tag{14}$$

Evidently, $\tilde{\boldsymbol{g}}(\boldsymbol{g}, \hat{\boldsymbol{g}})$ is invariant under the group action φ_{g_r}, i.e., $\tilde{\boldsymbol{g}}(\varphi_{g_r}(\boldsymbol{g}), \varphi_{g_r}(\hat{\boldsymbol{g}})) = \tilde{\boldsymbol{g}}(\boldsymbol{g}, \hat{\boldsymbol{g}})$. Note that the reference vectors $\boldsymbol{r}^i$, $i = 1, \cdots, n$ are expressed in the inertial frame. In addition, $\boldsymbol{q} \otimes (\hat{\boldsymbol{\beta}} - \boldsymbol{\beta}) \otimes \boldsymbol{q}^*$ couples the spacecraft attitude and transforms the bias error in the spacecraft body frame (i.e., $\hat{\boldsymbol{\beta}} - \boldsymbol{\beta}$) to the inertial frame. Therefore, the output error $\mathcal{E}(\hat{\boldsymbol{g}}, \boldsymbol{u}, \boldsymbol{y})$ and the bias estimation error $\tilde{\boldsymbol{\beta}}$ are both evaluated in the inertial frame.

B. Propagation and Updating Equations

With the invariant output error and estimation error defined in Eqs. (13) and (14), an IEKF based on discrete measurements is developed next. Note that the preceding output and state estimation errors are both induced by the group composition defined in Eq. (11), where the attitude quaternion $\boldsymbol{q}$ is multiplied on the right side by a unit quaternion $\boldsymbol{q}_r$. Hence, the derived IEKF is termed as right IEKF (RIEKF), following the terminology introduced in [25]. In the sequel, the subscript k indicates the value of a variable at time t_k. Define $\hat{\boldsymbol{g}}_k^- = (\hat{\boldsymbol{q}}_k^-, \hat{\boldsymbol{\beta}}_k^-) \in G$ as the a priori state estimate at time t_k just before, and $\hat{\boldsymbol{g}}_k^+ = (\hat{\boldsymbol{q}}_k^+, \hat{\boldsymbol{\beta}}_k^+) \in G$ the a posteriori state estimate after employing the measurement $\boldsymbol{y}_k = \boldsymbol{h}(\boldsymbol{g}_k, \boldsymbol{u}_k) + \boldsymbol{v}_k$ for correction.

The RIEKF is proposed with the following recursive propagation and update steps:

$$\dot{\hat{\boldsymbol{g}}} = \begin{pmatrix} \dot{\hat{\boldsymbol{q}}} \\ \dot{\hat{\boldsymbol{\beta}}} \end{pmatrix} = \begin{pmatrix} \frac{1}{2}\hat{\boldsymbol{q}} \otimes (\bar{\boldsymbol{\omega}} - \hat{\boldsymbol{\beta}}) \\ 0 \end{pmatrix}, \quad t_{k-1} \leq t < t_k \tag{15}$$

$$\hat{\boldsymbol{g}}_k^+ = \hat{\boldsymbol{g}}_k^- \circ [\exp_g(\boldsymbol{K}_k \mathcal{E}(\hat{\boldsymbol{g}}_k^-, \boldsymbol{u}_k, \boldsymbol{y}_k))]^{-1} \tag{16}$$

where $\hat{\boldsymbol{g}}_k^-$ is obtained by integrating Eq. (15) through the interval $[t_{k-1}, t_k)$ with the initial condition $\hat{\boldsymbol{g}}_{k-1}^+$; $\boldsymbol{K}_k \in \mathbb{R}^{6\times 3n}$ is the filter gain matrix to be designed later; $\exp_g(\cdot)$ is the exponential map from $\mathbb{R}^6$, which is identified with, or isomorphic to, the tangent space of G at $(\mathbf{1}, 0)$, to G. Letting

$$\begin{bmatrix} \boldsymbol{c}_k^q \\ \boldsymbol{c}_k^\beta \end{bmatrix} = \boldsymbol{K}_k \mathcal{E}(\hat{\boldsymbol{g}}_k^-, \boldsymbol{u}_k, \boldsymbol{y}_k), \quad \boldsymbol{c}_k^q, \boldsymbol{c}_k^\beta \in \mathbb{R}^3 \tag{17}$$

the function $\exp_g(\boldsymbol{K}_k \mathcal{E}(\hat{\boldsymbol{g}}_k^-, \boldsymbol{u}_k, \boldsymbol{y}_k))$ is then given by

$$\exp_g(\boldsymbol{K}_k \mathcal{E}(\hat{\boldsymbol{g}}_k^-, \boldsymbol{u}_k, \boldsymbol{y}_k)) = \exp_g \begin{pmatrix} \boldsymbol{c}_k^q \\ \boldsymbol{c}_k^\beta \end{pmatrix} = \begin{pmatrix} \exp_q\left(\frac{\boldsymbol{c}_k^q}{2}\right) \\ \boldsymbol{c}_k^\beta \end{pmatrix} \tag{18}$$

Evidently, the propagation equation of the RIEKF is identical to the classical quaternion MEKF. Even though the formalism of the update equation given in Eq. (16) is quite different from that of the MEKF, it is actually motivated by a philosophy similar to that behind the update step of the MEKF. More precisely, $\boldsymbol{K}_k \mathcal{E}(\hat{\boldsymbol{g}}_k^-, \boldsymbol{u}_k, \boldsymbol{y}_k)$ first produces a correction in the tangent space of the state manifold G from the measurement residual $\mathcal{E}(\hat{\boldsymbol{g}}_k^-, \boldsymbol{u}_k, \boldsymbol{y}_k)$. This correction is then transformed, herein by the exponential map $\exp_g(\cdot)$, onto the state manifold and $\exp_g(\boldsymbol{K}_k \mathcal{E}(\hat{\boldsymbol{g}}_k^-, \boldsymbol{u}_k, \boldsymbol{y}_k))$ is regarded as an estimate of the state error $\tilde{\boldsymbol{g}}$ at t_k. Since the state error defined in Eq. (14) implies $\boldsymbol{g} = \hat{\boldsymbol{g}} \circ \tilde{\boldsymbol{g}}^{-1}$, Eq. (16) is then derived by replacing $\hat{\boldsymbol{g}}$ and $\tilde{\boldsymbol{g}}$ with $\hat{\boldsymbol{g}}_k^-$ and $\exp_g(\boldsymbol{K}_k \mathcal{E}(\hat{\boldsymbol{g}}_k^-, \boldsymbol{u}_k, \boldsymbol{y}_k))$, respectively.

Note that $\exp_g(\boldsymbol{K}_k \mathcal{E}(\hat{\boldsymbol{g}}_k^-, \boldsymbol{u}_k, \boldsymbol{y}_k))$ is actually an element on G. Applying the inverse formula given in Eq. (12) to Eq. (18) and noting that $(\exp_q(\boldsymbol{c}_k^q/2))^* = \exp_q(-\boldsymbol{c}_k^q/2)$, one can derive

$$[\exp_g(\boldsymbol{K}_k \mathcal{E}(\hat{\boldsymbol{g}}_k^-, \boldsymbol{u}_k, \boldsymbol{y}_k))]^{-1} = \begin{pmatrix} \exp_q\left(-\frac{\boldsymbol{c}_k^q}{2}\right) \\ -\exp_q\left(\frac{\boldsymbol{c}_k^q}{2}\right) \otimes \boldsymbol{c}_k^\beta \otimes \exp_q\left(-\frac{\boldsymbol{c}_k^q}{2}\right) \end{pmatrix} \tag{19}$$

Substituting Eq. (19) into Eq. (16) and simple manipulations show that the update equation can be written as

$$\hat{\boldsymbol{g}}_k^+ = \begin{pmatrix} \hat{\boldsymbol{q}}_k^+ \\ \hat{\boldsymbol{\beta}}_k^+ \end{pmatrix} = \begin{pmatrix} \exp_q\left(-\frac{\boldsymbol{c}_k^q}{2}\right) \otimes \hat{\boldsymbol{q}}_k^- \\ \hat{\boldsymbol{\beta}}_k^- - (\hat{\boldsymbol{q}}_k^+)^* \otimes \boldsymbol{c}_k^\beta \otimes \hat{\boldsymbol{q}}_k^+ \end{pmatrix} \tag{20}$$

C. Filtering Gain Tuning

In this section, the filtering gain $\boldsymbol{K}_k$ is tuned based on the known sensor noise models. The estimation error equations are first computed and then linearized so that the standard Kalmam filter theory can be applied to obtain $\boldsymbol{K}_k$.

For $t \in [t_{k-1}, t_k)$, the propagation step is implemented and the governing equations of the estimation errors $\tilde{\boldsymbol{q}}$ and $\tilde{\boldsymbol{\beta}}$ are given by

$$\dot{\tilde{\boldsymbol{q}}} = -\frac{1}{2}\tilde{\boldsymbol{q}} \otimes \tilde{\boldsymbol{\beta}} + \frac{1}{2}\hat{\boldsymbol{\eta}}_v \otimes \tilde{\boldsymbol{q}} \tag{21}$$

$$\dot{\tilde{\boldsymbol{\beta}}} = [\boldsymbol{A}(\tilde{\boldsymbol{q}})(\hat{\boldsymbol{I}}_\omega - \hat{\boldsymbol{\eta}}_u)] \times \tilde{\boldsymbol{\beta}} - \boldsymbol{A}(\tilde{\boldsymbol{q}})\hat{\boldsymbol{\eta}}_u \tag{22}$$

where

$$\hat{\boldsymbol{\eta}}_v = \hat{\boldsymbol{q}} \otimes \boldsymbol{\eta}_v \otimes \hat{\boldsymbol{q}}^* = \boldsymbol{A}^T(\hat{\boldsymbol{q}})\boldsymbol{\eta}_v$$

$$\hat{\boldsymbol{I}}_\omega = \hat{\boldsymbol{q}} \otimes (\bar{\boldsymbol{\omega}} - \hat{\boldsymbol{\beta}}) \otimes \hat{\boldsymbol{q}}^* = \boldsymbol{A}^T(\hat{\boldsymbol{q}})(\bar{\boldsymbol{\omega}} - \hat{\boldsymbol{\beta}})$$

$$\hat{\boldsymbol{\eta}}_u = \hat{\boldsymbol{q}} \otimes \boldsymbol{\eta}_u \otimes \hat{\boldsymbol{q}}^* = \boldsymbol{A}^T(\hat{\boldsymbol{q}})\boldsymbol{\eta}_u$$

The details for deriving the above error dynamics are deferred to the Appendix.

From Eqs. (14) and (16), the a posteriori state estimation error at time t_k can be written as

$$\begin{aligned} \tilde{\boldsymbol{g}}_k^+ &= \boldsymbol{g}_k^{-1} \circ \hat{\boldsymbol{g}}_k^- \circ [\exp_g(\boldsymbol{K}_k \mathcal{E}(\hat{\boldsymbol{g}}_k^-, \boldsymbol{u}_k, \boldsymbol{y}_k))]^{-1} \\ &= \tilde{\boldsymbol{g}}_k^- \circ [\exp_g(\boldsymbol{K}_k \mathcal{E}(\hat{\boldsymbol{g}}_k^-, \boldsymbol{u}_k, \boldsymbol{y}_k))]^{-1} \end{aligned}$$

which, after employing Eq. (19), becomes

$$\begin{pmatrix} \tilde{\boldsymbol{q}}_k^+ \\ \tilde{\boldsymbol{\beta}}_k^+ \end{pmatrix} = \begin{pmatrix} \exp_q\left(-\frac{\boldsymbol{c}_k^q}{2}\right) \otimes \tilde{\boldsymbol{q}}_k^- \\ \tilde{\boldsymbol{\beta}}^- - (\tilde{\boldsymbol{q}}_k^+)^* \otimes \boldsymbol{c}_k^\beta \otimes \tilde{\boldsymbol{q}}_k^+ \end{pmatrix} = \begin{pmatrix} \exp_q\left(-\frac{\boldsymbol{c}_k^q}{2}\right) \otimes \tilde{\boldsymbol{q}}_k^- \\ \tilde{\boldsymbol{\beta}}^- - \boldsymbol{A}(\tilde{\boldsymbol{q}}_k^+)\boldsymbol{c}_k^\beta \end{pmatrix} \tag{23}$$

Next, Eqs. (21), (22) and (23) are linearized by assuming that the estimation error and noise are both small. In other words, $\tilde{\boldsymbol{g}}$ is close to the identity element $(\boldsymbol{1}, 0)$ and $\|\boldsymbol{\eta}_v\|, \|\boldsymbol{\eta}_u\|, \|\boldsymbol{V}\| \ll 1$. Denote by $\tilde{\boldsymbol{\gamma}} \in \mathbb{R}^3$ the principal rotation vector corresponding to $\tilde{\boldsymbol{q}}$, that is

$$\tilde{\boldsymbol{q}} = \exp_q\left(\frac{\tilde{\boldsymbol{\gamma}}}{2}\right) = \begin{bmatrix} \cos\left(\frac{\|\tilde{\boldsymbol{\gamma}}\|}{2}\right) \\ \frac{\tilde{\boldsymbol{\gamma}}}{\|\tilde{\boldsymbol{\gamma}}\|}\sin\left(\frac{\|\tilde{\boldsymbol{\gamma}}\|}{2}\right) \end{bmatrix}$$

The small error assumption then implies $\|\tilde{\boldsymbol{\gamma}}\| \ll 1$ and $\tilde{\boldsymbol{q}} \approx [1, (\tilde{\boldsymbol{\gamma}}/2)^T]^T$. Substituting $[1, (\tilde{\boldsymbol{\gamma}}/2)^T]^T$ for $\tilde{\boldsymbol{q}}$ in Eq. (21), applying the quaternion product, and retaining the first-order terms, one can readily obtain

$$\dot{\tilde{\boldsymbol{\gamma}}} = \tilde{\boldsymbol{\beta}} - \hat{\boldsymbol{\eta}}_v \tag{24}$$

Note that

$$\boldsymbol{A}(\tilde{\boldsymbol{q}}) \approx \boldsymbol{I}_3 - \tilde{\boldsymbol{\gamma}}^{\times}$$

Employing the above approximation and omitting the second-order terms such as $(\tilde{\boldsymbol{\gamma}}^{\times}\hat{\boldsymbol{I}}_{\omega}) \times \tilde{\boldsymbol{\beta}}$ and $\tilde{\boldsymbol{\gamma}}^{\times}\hat{\boldsymbol{\eta}}_u$, the linearization of Eq. (22) is computed as

$$\dot{\tilde{\boldsymbol{\beta}}} = \hat{\boldsymbol{I}}_{\omega} \times \tilde{\boldsymbol{\beta}} - \hat{\boldsymbol{\eta}}_u \tag{25}$$

Equations (24) and (25) can be formulated in the matrix form

$$\begin{bmatrix} \dot{\tilde{\boldsymbol{\gamma}}} \\ \dot{\tilde{\boldsymbol{\beta}}} \end{bmatrix} = \boldsymbol{F} \begin{bmatrix} \tilde{\boldsymbol{\gamma}} \\ \tilde{\boldsymbol{\beta}} \end{bmatrix} + \boldsymbol{G} \begin{bmatrix} \boldsymbol{\eta}_v \\ \boldsymbol{\eta}_u \end{bmatrix} \tag{26}$$

where

$$\begin{gathered} \boldsymbol{F} = \begin{bmatrix} \boldsymbol{0}_{3\times3} & -\boldsymbol{I}_3 \\ \boldsymbol{0}_{3\times3} & \hat{\boldsymbol{I}}_{\omega}^{\times} \end{bmatrix}, \quad \boldsymbol{G} = \begin{bmatrix} \boldsymbol{A}^T(\hat{\boldsymbol{q}}) & \boldsymbol{0}_{3\times3} \\ \boldsymbol{0}_{3\times3} & -\boldsymbol{A}^T(\hat{\boldsymbol{q}}) \end{bmatrix} \\ \boldsymbol{Q} = E\left\{ \begin{bmatrix} \boldsymbol{\eta}_v \\ \boldsymbol{\eta}_u \end{bmatrix} [\boldsymbol{\eta}_v^T, \boldsymbol{\eta}_u^T] \right\} = \begin{bmatrix} \sigma_v^2 \boldsymbol{I}_3 & \boldsymbol{0}_{3\times3} \\ \boldsymbol{0}_{3\times3} & \sigma_u^2 \boldsymbol{I}_3 \end{bmatrix} \end{gathered} \tag{27}$$

The small estimation error also implies that the correction $(\boldsymbol{c}_k^q, \boldsymbol{c}_k^{\beta})$ is small. The first-order approximations for $\tilde{\boldsymbol{q}}_k^+$, $\tilde{\boldsymbol{q}}_k^-$, and $\exp_q(\boldsymbol{c}_k^q/2)$ are given by $[1, (\tilde{\boldsymbol{\gamma}}_k^+/2)^T]^T$, $[1, (\tilde{\boldsymbol{\gamma}}_k^-/2)^T]^T$, and

$[1, (\boldsymbol{c}_k^q/2)^T]^T$, respectively. Substituting these approximations into Eq. (23) and keeping the first-order terms leads to

$$\begin{bmatrix} \tilde{\boldsymbol{\gamma}}_k^+ \\ \tilde{\boldsymbol{\beta}}_k^+ \end{bmatrix} = \begin{bmatrix} \tilde{\boldsymbol{\gamma}}_k^- \\ \tilde{\boldsymbol{\beta}}_k^- \end{bmatrix} - \begin{bmatrix} \boldsymbol{c}_k^q \\ \boldsymbol{c}_k^\beta \end{bmatrix} \tag{28}$$

According to Eq. (13), the invariant output error at time t_k is given by

$$\mathcal{E}(\hat{\boldsymbol{g}}_k^-, \boldsymbol{u}_k, \boldsymbol{y}_k) = \begin{bmatrix} \boldsymbol{r}_k^1 \\ \vdots \\ \boldsymbol{r}_k^n \end{bmatrix} - \begin{bmatrix} \hat{\boldsymbol{q}}_k^- \otimes \boldsymbol{y}_k^1 \otimes (\hat{\boldsymbol{q}}_k^-)^* \\ \vdots \\ \hat{\boldsymbol{q}}_k^- \otimes \boldsymbol{y}_k^n \otimes (\hat{\boldsymbol{q}}_k^-)^* \end{bmatrix} \tag{29}$$

Since $\boldsymbol{y}_k^i = \boldsymbol{q}_k^* \otimes \boldsymbol{r}_k^i \otimes \boldsymbol{q}_k + \boldsymbol{v}_k^i$, $i = 1, \cdots, n$, it follows that

$$\begin{aligned} \hat{\boldsymbol{q}}_k^- \otimes \boldsymbol{y}_k^i \otimes (\hat{\boldsymbol{q}}_k^-)^* &= \tilde{\boldsymbol{q}}_k^- \otimes \boldsymbol{r}_k^i \otimes (\tilde{\boldsymbol{q}}_k^-)^* + \hat{\boldsymbol{q}}_k^- \otimes \boldsymbol{v}_k^i \otimes (\hat{\boldsymbol{q}}_k^-)^* \\ &= \boldsymbol{A}^T(\tilde{\boldsymbol{q}}_k^-)\boldsymbol{r}_k^i + \boldsymbol{A}^T(\hat{\boldsymbol{q}}_k^-)\boldsymbol{v}_k^i \\ &\approx (\boldsymbol{I}_3 + \tilde{\boldsymbol{\gamma}}_k^\times)\boldsymbol{r}_k^i + \boldsymbol{A}^T(\hat{\boldsymbol{q}}_k^-)\boldsymbol{v}_k^i \end{aligned}$$

Consequently, the linearization of Eq. (29) is derived as

$$\mathcal{E}(\hat{\boldsymbol{g}}_k^-, \boldsymbol{u}_k, \boldsymbol{y}_k) = \boldsymbol{H}_k \begin{bmatrix} \tilde{\boldsymbol{\gamma}}_k^- \\ \tilde{\boldsymbol{\beta}}_k^- \end{bmatrix} + \hat{\boldsymbol{V}}_k \tag{30}$$

where

$$\boldsymbol{H}_k = \begin{bmatrix} (\boldsymbol{r}_k^1)^\times & \boldsymbol{0}_{3\times 3} \\ \vdots & \vdots \\ (\boldsymbol{r}_k^n)^\times & \boldsymbol{0}_{3\times 3} \end{bmatrix}, \quad \hat{\boldsymbol{V}}_k = \begin{bmatrix} \boldsymbol{A}^T(\hat{\boldsymbol{q}}_k^-) & & \boldsymbol{0}_{3\times 3} \\ & \ddots & \\ \boldsymbol{0}_{3\times 3} & & \boldsymbol{A}^T(\hat{\boldsymbol{q}}_k^-) \end{bmatrix} \boldsymbol{V}_k \tag{31}$$

Substitution of Eq. (17) into Eq. (28) and invoking Eq. (30), it follows that

$$\begin{bmatrix} \tilde{\boldsymbol{\gamma}}_k^+ \\ \tilde{\boldsymbol{\beta}}_k^+ \end{bmatrix} = (\boldsymbol{I}_6 - \boldsymbol{K}_k\boldsymbol{H}_k) \begin{bmatrix} \tilde{\boldsymbol{\gamma}}_k^- \\ \tilde{\boldsymbol{\beta}}_k^- \end{bmatrix} - \boldsymbol{K}_k\hat{\boldsymbol{V}}_k \tag{32}$$

Applying the Kalman filter design to the linearized system given in Eqs (26) and (32), the filtering gain $\boldsymbol{K}_k$ and the estimation error covariance $\boldsymbol{P}_k^+$ are then computed as follows

$$\begin{aligned} \dot{\boldsymbol{P}} &= \boldsymbol{F}\boldsymbol{P} + \boldsymbol{P}\boldsymbol{F}^T + \boldsymbol{G}\boldsymbol{Q}\boldsymbol{G}^T, \quad t_{k-1} \le t < t_k \\ \boldsymbol{P}_k^+ &= (\boldsymbol{I}_6 - \boldsymbol{K}_k\boldsymbol{H}_k)\boldsymbol{P}_k^- \\ \boldsymbol{K}_k &= \boldsymbol{P}_k^-\boldsymbol{H}_k^T(\boldsymbol{H}_k\boldsymbol{P}_k^-\boldsymbol{H}_k^T + \hat{\boldsymbol{R}}_k)^{-1} \end{aligned} \tag{33}$$

where $\boldsymbol{P}_k^-$ is obtained by integrating $\dot{\boldsymbol{P}}$ through the interval $[t_{k-1}, t_k)$ with the initial condition $\boldsymbol{P}_{k-1}^+$, and $\hat{\boldsymbol{R}}_k$ is given by

$$\hat{\boldsymbol{R}}_k = E\{\hat{\boldsymbol{V}}_k\hat{\boldsymbol{V}}_k^T\} = \begin{bmatrix} \boldsymbol{A}^T(\hat{\boldsymbol{q}}_k^-) & & \boldsymbol{0}_{3\times3} \\ & \ddots & \\ \boldsymbol{0}_{3\times3} & & \boldsymbol{A}^T(\hat{\boldsymbol{q}}_k^-) \end{bmatrix} \boldsymbol{R}_k \begin{bmatrix} \boldsymbol{A}(\hat{\boldsymbol{q}}_k^-) & & \boldsymbol{0}_{3\times3} \\ & \ddots & \\ \boldsymbol{0}_{3\times3} & & \boldsymbol{A}(\hat{\boldsymbol{q}}_k^-) \end{bmatrix} \tag{34}$$

D. Summary of the RIEKF Algorithm

Finally, the RIEKF algorithm is described as follows:

$$\text{Initialize: } \hat{\boldsymbol{q}}_0 = \hat{\boldsymbol{q}}(t_0), \hat{\boldsymbol{\beta}}_0 = \hat{\boldsymbol{\beta}}(t_0), \boldsymbol{P}_0 = \boldsymbol{P}(t_0)$$

$$\text{Propagation: } \begin{cases} \dot{\hat{\boldsymbol{q}}} &= \frac{1}{2}\hat{\boldsymbol{q}} \otimes (\bar{\boldsymbol{\omega}} - \hat{\boldsymbol{\beta}}) \\ \dot{\hat{\boldsymbol{\beta}}} &= 0 \\ \dot{\boldsymbol{P}} &= \boldsymbol{F}\boldsymbol{P} + \boldsymbol{P}\boldsymbol{F}^T + \boldsymbol{G}\boldsymbol{Q}\boldsymbol{G}^T \end{cases}$$

$$\text{Update: } \begin{cases} \boldsymbol{K}_k &= \boldsymbol{P}_k^-\boldsymbol{H}_k^T(\boldsymbol{H}_k\boldsymbol{P}_k^-\boldsymbol{H}_k^T + \hat{\boldsymbol{R}}_k)^{-1} \\ \boldsymbol{P}_k^+ &= (\boldsymbol{I}_6 - \boldsymbol{K}_k\boldsymbol{H}_k)\boldsymbol{P}_k^- \\ \begin{bmatrix} \boldsymbol{c}_k^q \\ \boldsymbol{c}_k^\beta \end{bmatrix} &= \boldsymbol{K}_k\mathcal{E}(\hat{\boldsymbol{g}}_k^-, \boldsymbol{u}_k, \boldsymbol{y}_k) \\ \hat{\boldsymbol{q}}_k^+ &= \exp_q\left(-\frac{\boldsymbol{c}_k^q}{2}\right) \otimes \hat{\boldsymbol{q}}_k^- \\ \hat{\boldsymbol{\beta}}_k^+ &= \hat{\boldsymbol{\beta}}_k^- - (\hat{\boldsymbol{q}}_k^+)^* \otimes \boldsymbol{c}_k^\beta \otimes \hat{\boldsymbol{q}}_k^+ \\ \hat{\boldsymbol{\omega}}_k^+ &= \bar{\boldsymbol{\omega}}_k - \hat{\boldsymbol{\beta}}_k^+ \end{cases}$$

where the matrices $\boldsymbol{F}$, $\boldsymbol{G}$, and $\boldsymbol{Q}$ are given in Eq. (27); $\mathcal{E}(\hat{\boldsymbol{g}}_k^-, \boldsymbol{u}_k, \boldsymbol{y}_k)$, $\boldsymbol{H}_k$ and $\hat{\boldsymbol{R}}_k$ are given in Eqs. (29), (31) and (34) respectively.

IV. Left Invariant Extended Kalman Filter Design

The preceding quaternion RIEKF roots in the group structure of the state space given by Eq. (11). In fact, $G = \mathbb{S}^3 \times \mathbb{R}^3$ remains a Lie group with the identity element $(\mathbf{1}, 0) \in G$ if endowed with the following alternative binary composition:

$$\boldsymbol{g}_r \circ \boldsymbol{g} = \begin{pmatrix} \boldsymbol{q}_r \\ \boldsymbol{\beta}_r \end{pmatrix} \circ \begin{pmatrix} \boldsymbol{q} \\ \boldsymbol{\beta} \end{pmatrix} = \begin{pmatrix} \boldsymbol{q}_r \otimes \boldsymbol{q} \\ \boldsymbol{\beta}_r + \boldsymbol{\beta} \end{pmatrix} \tag{35}$$

where $\boldsymbol{g}_r = (\boldsymbol{q}_r, \boldsymbol{\beta}_r), \boldsymbol{g} = (\boldsymbol{q}, \boldsymbol{\beta}) \in G$. The inverse of $\boldsymbol{g}$ becomes $\boldsymbol{g}^{-1} = (\boldsymbol{q}^*, -\boldsymbol{\beta})$. In contrast to Eq. (11), the attitude quaternion $\boldsymbol{q}$ is now multiplied on the left side by the unit quaternion $\boldsymbol{q}_r$ in the group composition given by Eq. (35), which can be utilized to derive a left IEKF (LIEKF) in a manner similar to Section III.

To this end, redefine the group actions on the state space and input space of system (9) as

$$\begin{aligned} \varphi_{g_r}(\boldsymbol{g}) &= \boldsymbol{g}_r \circ \boldsymbol{g} \\ \psi_{g_r}(\boldsymbol{u}) &= (\bar{\boldsymbol{\omega}} + \boldsymbol{\beta}_r, \boldsymbol{q}_r \otimes \boldsymbol{r}^1 \otimes \boldsymbol{q}_r^*, \cdots, \boldsymbol{q}_r \otimes \boldsymbol{r}^n \otimes \boldsymbol{q}_r^*) \end{aligned}$$

which give rise to the identity map $\rho_{g_r} = \mathrm{Id}$ acting on the output space such that

$$\rho_{g_r} \boldsymbol{h}(\boldsymbol{g}, \boldsymbol{u}) = \boldsymbol{h}(\varphi_{g_r}(\boldsymbol{g}), \psi_{g_r}(\boldsymbol{u})) = \boldsymbol{h}(\boldsymbol{g}, \boldsymbol{u})$$

It is then direct to verify by virtue of Definitions 1 and 2 that system (9) is G-invariant with G-equivariant output with respect to the above φ_{g_r}, ψ_{g_r}, and ρ_{g_r}. Letting $\hat{\boldsymbol{g}} = (\hat{\boldsymbol{q}}, \hat{\boldsymbol{\beta}}) \in G$ be the estimate of $\boldsymbol{g}$, these group actions induce the following invariant output error and invariant estimation error:

$$\begin{aligned}\mathcal{E}(\hat{\boldsymbol{g}},\boldsymbol{u},\boldsymbol{y}) &= \rho_{\hat{g}^{-1}}(\boldsymbol{y}) - \rho_{\hat{g}^{-1}}(\boldsymbol{h}(\hat{\boldsymbol{g}},\boldsymbol{u})) \\ &= \boldsymbol{y} - \boldsymbol{h}(\hat{\boldsymbol{g}},\boldsymbol{u}) = \boldsymbol{y} - \begin{bmatrix} \hat{\boldsymbol{q}}^* \otimes \boldsymbol{r}^1 \otimes \hat{\boldsymbol{q}} \\ \vdots \\ \hat{\boldsymbol{q}}^* \otimes \boldsymbol{r}^n \otimes \hat{\boldsymbol{q}} \end{bmatrix}\end{aligned} \tag{36}$$

$$\tilde{\boldsymbol{g}}(\boldsymbol{g},\hat{\boldsymbol{g}}) = \begin{pmatrix} \tilde{\boldsymbol{q}} \\ \tilde{\boldsymbol{\beta}} \end{pmatrix} = \hat{\boldsymbol{g}}^{-1} \circ \boldsymbol{g} = \begin{pmatrix} \hat{\boldsymbol{q}}^* \otimes \boldsymbol{q} \\ \boldsymbol{\beta} - \hat{\boldsymbol{\beta}} \end{pmatrix} \tag{37}$$

Clearly, the above output error and bias error are both evaluated in the spacecraft body frame. In addition, the attitude error and bias error are defined in a decoupled manner.

The continuous-discrete quaternion LIEKF is constructed with the same propagation step as Eq. (15) and the updating step

$$\hat{\boldsymbol{g}}_k^+ = \hat{\boldsymbol{g}}_k^- \circ \exp_g(\boldsymbol{K}_k(\boldsymbol{y}_k - \boldsymbol{h}(\hat{\boldsymbol{g}}_k^-, \boldsymbol{u}_k)))$$

where $\boldsymbol{K}_k \in \mathbb{R}^{6\times 3n}$ and $\boldsymbol{c}_k^q \in \mathbb{R}^3$ and $\boldsymbol{c}_k^\beta \in \mathbb{R}^3$ are now given by

$$\begin{bmatrix} \boldsymbol{c}_k^q \\ \boldsymbol{c}_k^\beta \end{bmatrix} = \boldsymbol{K}_k(\boldsymbol{y}_k - \boldsymbol{h}(\hat{\boldsymbol{g}}_k^-, \boldsymbol{u}_k))$$

Further algebraic manipulations show that the updating step is equivalent to

$$\begin{pmatrix} \hat{\boldsymbol{q}}_k^+ \\ \hat{\boldsymbol{\beta}}_k^+ \end{pmatrix} = \begin{pmatrix} \hat{\boldsymbol{q}}_k^- \otimes \exp_q\left(\frac{\boldsymbol{c}_k^q}{2}\right) \\ \hat{\boldsymbol{\beta}}_k^- + \boldsymbol{c}_k^\beta \end{pmatrix}$$

In addition, the estimation error equation and the a posteriori estimation error are derived as

$$\begin{cases} \dot{\tilde{\boldsymbol{q}}} &= \frac{1}{2}\tilde{\boldsymbol{q}} \otimes ([\boldsymbol{A}(\tilde{\boldsymbol{q}}) - \boldsymbol{I}_3](\bar{\boldsymbol{\omega}} - \hat{\boldsymbol{\beta}}) - \tilde{\boldsymbol{\beta}} - \boldsymbol{\eta}_v) \\ \dot{\tilde{\boldsymbol{\beta}}} &= \boldsymbol{\eta}_u \end{cases} \tag{38}$$

$$\begin{pmatrix} \tilde{\boldsymbol{q}}_k^+ \\ \tilde{\boldsymbol{\beta}}_k^+ \end{pmatrix} = \begin{pmatrix} \exp_q\left(-\frac{\boldsymbol{c}_k^q}{2}\right) \otimes \tilde{\boldsymbol{q}}_k^- \\ \tilde{\boldsymbol{\beta}}^- - \boldsymbol{c}_k^\beta \end{pmatrix} \tag{39}$$

Similarly to the RIEKF, the filtering gain $\boldsymbol{K}_k$ is tuned by applying the Kalman equations to the linearization of Eqs. (38) and (39). Derivations analogous to those in Section III.C produce the following quaternion LIEKF algorithm:

$$\text{Initialize: } \hat{\boldsymbol{q}}_0 = \hat{\boldsymbol{q}}(t_0), \hat{\boldsymbol{\beta}}_0 = \hat{\boldsymbol{\beta}}(t_0), \boldsymbol{P}_0 = \boldsymbol{P}(t_0)$$

$$\text{Propagation: } \begin{cases} \dot{\hat{\boldsymbol{q}}} &= \frac{1}{2}\hat{\boldsymbol{q}} \otimes (\bar{\boldsymbol{\omega}} - \hat{\boldsymbol{\beta}}) \\ \dot{\hat{\boldsymbol{\beta}}} &= 0 \\ \dot{\boldsymbol{P}} &= \boldsymbol{F}\boldsymbol{P} + \boldsymbol{P}\boldsymbol{F}^T + \boldsymbol{G}\boldsymbol{Q}\boldsymbol{G}^T \end{cases}$$

$$\text{Update: } \begin{cases} \boldsymbol{K}_k &= \boldsymbol{P}_k^- \boldsymbol{H}_k^T (\boldsymbol{H}_k \boldsymbol{P}_k^- \boldsymbol{H}_k^T + \boldsymbol{R}_k)^{-1} \\ \boldsymbol{P}_k^+ &= (\boldsymbol{I}_6 - \boldsymbol{K}_k \boldsymbol{H}_k)\boldsymbol{P}_k^- \\ \begin{bmatrix} \boldsymbol{c}_k^q \\ \boldsymbol{c}_k^\beta \end{bmatrix} &= \boldsymbol{K}_k(\boldsymbol{y}_k - \boldsymbol{h}(\hat{\boldsymbol{g}}_k^-, \boldsymbol{u}_k)) \\ \hat{\boldsymbol{q}}_k^+ &= \hat{\boldsymbol{q}}_k^- \otimes \exp_q\left(\frac{\boldsymbol{c}_k^q}{2}\right) \\ \hat{\boldsymbol{\beta}}_k^+ &= \hat{\boldsymbol{\beta}}_k^- + \boldsymbol{c}_k^\beta \\ \hat{\boldsymbol{\omega}}_k^+ &= \bar{\boldsymbol{\omega}}_k - \hat{\boldsymbol{\beta}}_k^+ \end{cases}$$

where $\boldsymbol{Q}$ remains the same as that given in Eq. (27) while $\boldsymbol{F}$, $\boldsymbol{G}$, and $\boldsymbol{H}_k$ are given by

$$\boldsymbol{F} = \begin{bmatrix} -(\bar{\boldsymbol{\omega}} - \hat{\boldsymbol{\beta}})^\times & -\boldsymbol{I}_3 \\ \boldsymbol{0}_{3\times3} & \boldsymbol{0}_{3\times3} \end{bmatrix}, \quad \boldsymbol{G} = \begin{bmatrix} -\boldsymbol{I}_3 & \boldsymbol{0}_{3\times3} \\ \boldsymbol{0}_{3\times3} & \boldsymbol{I}_3 \end{bmatrix}$$

$$\boldsymbol{H}_k = \begin{bmatrix} (\boldsymbol{A}(\hat{\boldsymbol{q}}_k^-)\boldsymbol{r}_k^1)^\times & \boldsymbol{0}_{3\times3} \\ \vdots & \vdots \\ (\boldsymbol{A}(\hat{\boldsymbol{q}}_k^-)\boldsymbol{r}_k^n)^\times & \boldsymbol{0}_{3\times3} \end{bmatrix}$$

V. Discussion

Next, the similarities and differences between the RIEKF, LIEKF, and MEKF as well as their indications are discussed.

It is not a surprise that the quaternion LIEKF is mostly identical to the conventional quaternion MEKF [31] except the attitude correction step, because they are derived from the same output-state errors (Note that the quaternion product defined in this paper is different that adopted in [31]). In other words, they share the same invariance property induced by the state-space group structure defined in Eq. (35). The quaternion LIEKF generates a unit quaternion for correction via the quaternion exponential map and thus respects the unit-quaternion norm constraint naturally. The quaternion MEKF, however, utilizes the first-order approximation $[1, (\boldsymbol{c}_k^q/2)^T]^T$ for correction and requires a brute-force normalization to ensure $\hat{\boldsymbol{q}}_k^+ \in \mathbb{S}^3$ [31]. Nonetheless, this difference is minor and hence the quaternion MEKF can be viewed as a minor variant of the quaternion LIEKF. It can be expected that they have similar performance at most times, as shown by the substantial numerical simulations in Section VI. The above observation thus casts insight to the quaternion MEKF from the perspective of invariant Kalman filtering theory.

Although the RIEKF and LIEKF (and MEKF) share the same dynamics predicting $(\hat{\boldsymbol{q}}, \hat{\boldsymbol{\beta}})$, their covariance and Kalman gain computations and update equations are different. More precisely, the RIEKF and LIEKF involve different $\boldsymbol{F}$, $\boldsymbol{G}$, and $\boldsymbol{H}_k$ matrices. In addition, the effect of vector measurement noise is taken into account by $\hat{\boldsymbol{R}}_k$ in the RIEKF but by $\boldsymbol{R}_k$ in the LIEKF. The difference roots in their different dependence on the estimated state trajectory, as can be observed from their respective algorithms and estimation error equations, namely, Eqs. (21) and (22) for the RIEKF, and Eq. (38) for the LIEKF:

1) The noise processes $\hat{\boldsymbol{\eta}}_v$ and $\hat{\boldsymbol{\eta}}_u$ in Eqs. (21) and (22) are dependent on the attitude estimate $\hat{\boldsymbol{q}}$ while $\boldsymbol{\eta}_v$ and $\boldsymbol{\eta}_u$ in Eq. (38) are not. Since $\hat{\boldsymbol{\eta}}_v$ and $\hat{\boldsymbol{\eta}}_u$ relate respectively to $\boldsymbol{\eta}_v$ and $\boldsymbol{\eta}_u$ via a $\hat{\boldsymbol{q}}$-dependent coordinate transformation, they have the same magnitude as, and their influence on the estimation error system is similar to that of $\boldsymbol{\eta}_v$ and $\boldsymbol{\eta}_u$. Actually, since the gyro noise is assumed to be isotropic and $\boldsymbol{Q}$ takes the form as given in Eq. (27), it follows that the term $\boldsymbol{GQG}$ in the RIEKF is equal to that in the LIEKF and they both reduce to $\boldsymbol{Q}$. Similarly, if the measurement noise is also isotropic (i.e., $\boldsymbol{R}_k^{ij} = \boldsymbol{0}_{3\times 3}$ for $i \neq j$ and $\boldsymbol{R}_k^{ii}$ is diagonal with equal diagonal entries), then $\hat{\boldsymbol{R}}_k$ in the RIEKF reduces to $\boldsymbol{R}_k$ in the LIEKF. The above observation implies that for the RIEKF and LIEKF the statistical properties of the system noise and measurement noise have nearly

the same effect in propagating the respective $\boldsymbol{P}_k$ and $\boldsymbol{K}_k$.

2) Turning off the noise in Eqs. (21), (22) and (38), we obtain

$$\text{RIEKF:} \begin{cases} \dot{\tilde{\boldsymbol{q}}} &= -\frac{1}{2}\tilde{\boldsymbol{q}} \otimes \tilde{\boldsymbol{\beta}} \\ \dot{\tilde{\boldsymbol{\beta}}} &= (\boldsymbol{A}(\tilde{\boldsymbol{q}})\hat{\boldsymbol{I}}_\omega) \times \tilde{\boldsymbol{\beta}} \end{cases}$$

$$\text{LIEKF:} \begin{cases} \dot{\tilde{\boldsymbol{q}}} &= \frac{1}{2}\tilde{\boldsymbol{q}} \otimes ([\boldsymbol{A}(\tilde{\boldsymbol{q}}) - \boldsymbol{I}_3](\bar{\boldsymbol{\omega}} - \hat{\boldsymbol{\beta}}) - \tilde{\boldsymbol{\beta}}) \\ \dot{\tilde{\boldsymbol{\beta}}} &= 0 \end{cases}$$

As can be seen from the above noise-free error equations, the key variable characterizing the dependence of the RIEKF on the estimated trajectory and input is $\hat{\boldsymbol{I}}_\omega = \boldsymbol{A}^T(\hat{\boldsymbol{q}})(\bar{\boldsymbol{\omega}} - \hat{\boldsymbol{\beta}})$ while that of the LIEKF is $\bar{\boldsymbol{\omega}} - \hat{\boldsymbol{\beta}}$. For the RIEKF, $\hat{\boldsymbol{I}}_\omega$ appears only in the bias error equation and does not influence the attitude error equation directly. In contrast, $\bar{\boldsymbol{\omega}} - \hat{\boldsymbol{\beta}}$ does not appear in the bias error equation of the LIEKF but directly affects its attitude error equation. Accordingly, this difference leads to dramatically different $\boldsymbol{F}$ matrices for the RIEKF and LIEKF. Given that the bias is nearly constant and the bias error is slowly varying, the RIEKF actually restricts the dependence on the trajectory and input to a slowly varying state error. Moreover, the sensitivity matrix $\boldsymbol{H}_k$ of the RIEKF does not depend on the estimated attitude but that of the LIEKF does. Therefore, the RIEKF has less dependence on the estimated trajectory and input, and its performance is more robust to initial estimation errors, than the LIEKF (and also the MEKF).

The physical difference between the RIEKF and LIEKF (and MEKF) can be obtained by further inspecting the invariant output errors and state estimation errors, from which they are derived. The attitude error in the LIEKF (and MEKF) has a clear physical meaning and can be viewed as the attitude error in the spacecraft body frame $\mathcal{F}_B$. In contrast, the physical meaning of the attitude error in the RIEKF is not straight to see. It would be interesting to find the relationship between these two attitude errors. To this end, denote by

$$\exp_q\left(\frac{\tilde{\boldsymbol{\gamma}}_I}{2}\right) = \hat{\boldsymbol{q}} \otimes \boldsymbol{q}^*, \quad \exp_q\left(\frac{\tilde{\boldsymbol{\gamma}}_B}{2}\right) = \hat{\boldsymbol{q}}^* \otimes \boldsymbol{q}$$

where the subscripts I and B are used to distinguish the principal rotation vectors corresponding

to the two error quaternions. Note that $\hat{\boldsymbol{q}}$ gives an estimated spacecraft frame, which can be denoted as $\mathcal{F}_E$. Then, $\hat{\boldsymbol{q}}^* \otimes \boldsymbol{q}$ represents the attitude quaternion of $\mathcal{F}_B$ relative to $\mathcal{F}_E$. Hence, $\tilde{\boldsymbol{\gamma}}_I$ is the principal rotation vector that brings $\mathcal{F}_E$ to $\mathcal{F}_B$ and has the same components in both frames. In this sense, $\hat{\boldsymbol{q}}^* \otimes \boldsymbol{q}$ is viewed as the attitude error in the spacecraft body frame. Noting $\hat{\boldsymbol{q}} = (\exp_q(\tilde{\boldsymbol{\gamma}}_B/2) \otimes \boldsymbol{q}^*)^* = \boldsymbol{q} \otimes \exp_q(-\tilde{\boldsymbol{\gamma}}_B/2)$, it follows that

$$\exp_q\left(\frac{\tilde{\boldsymbol{\gamma}}_I}{2}\right) = \boldsymbol{q} \otimes \exp_q\left(-\frac{\tilde{\boldsymbol{\gamma}}_B}{2}\right) \otimes \boldsymbol{q}^* = \exp_q\left(-\frac{\boldsymbol{q} \otimes \tilde{\boldsymbol{\gamma}}_B \otimes \boldsymbol{q}^*}{2}\right)$$

where Eq. (4) is employed to derive the second equality. It is then straight to see that

$$\tilde{\boldsymbol{\gamma}}_I = -\boldsymbol{q} \otimes \tilde{\boldsymbol{\gamma}}_B \otimes \boldsymbol{q}^* = -\boldsymbol{A}^T(\boldsymbol{q})\tilde{\boldsymbol{\gamma}}_B$$

Since $\boldsymbol{A}^T(\boldsymbol{q})$ is the rotation matrix from $\mathcal{F}_B$ to the inertial frame $\mathcal{F}_I$ and $\tilde{\boldsymbol{\gamma}}_B$ is given in $\mathcal{F}_B$, $\tilde{\boldsymbol{\gamma}}_I$ is actually the inertial representation of $-\tilde{\boldsymbol{\gamma}}_B$, the principal rotation vector that brings $\mathcal{F}_B$ to $\mathcal{F}_E$. In this sense, $\hat{\boldsymbol{q}} \otimes \boldsymbol{q}^*$ can be viewed as the attitude estimation error in the inertial frame. Recall that the output error and bias error defined in Eqs. (13) and (14) are both evaluated in the inertial frame. Therefore, the RIEKF builds on invariant output errors and state estimation errors in the inertial frame. Conversely, the LIEKF (and MEKF) builds on invariant output errors and state estimation errors in the body frame. The above is the physical insight underlying the RIEKF, LIEKF and MEKF. Additionally, letting $\tilde{\boldsymbol{\beta}}_B = \boldsymbol{\beta} - \hat{\boldsymbol{\beta}}$ and $\tilde{\boldsymbol{\beta}}_I = \boldsymbol{A}^T(\boldsymbol{q})(\hat{\boldsymbol{\beta}} - \boldsymbol{\beta})$, the estimation error covariance for the RIEKF is related to that for the LIEKF by

$$E\left\{\begin{bmatrix}\tilde{\boldsymbol{\gamma}}_B \\ \tilde{\boldsymbol{\beta}}_B\end{bmatrix}[\tilde{\boldsymbol{\gamma}}_B^T, \tilde{\boldsymbol{\beta}}_B^T]\right\} = \begin{bmatrix}\boldsymbol{A}(\boldsymbol{q}) & \boldsymbol{0}_{3\times3} \\ \boldsymbol{0}_{3\times3} & \boldsymbol{A}(\boldsymbol{q})\end{bmatrix} E\left\{\begin{bmatrix}\tilde{\boldsymbol{\gamma}}_I \\ \tilde{\boldsymbol{\beta}}_I\end{bmatrix}[\tilde{\boldsymbol{\gamma}}_I^T, \tilde{\boldsymbol{\beta}}_I^T]\right\} \begin{bmatrix}\boldsymbol{A}^T(\boldsymbol{q}) & \boldsymbol{0}_{3\times3} \\ \boldsymbol{0}_{3\times3} & \boldsymbol{A}^T(\boldsymbol{q})\end{bmatrix} \tag{40}$$

Note that this is not the first time that attitude errors expressed in the inertial frame are applied for attitude estimation. An early application was previously proposed by Gai et al. [32]. The error quaternion defined there, however, is the conjugate of that for the RIEKF. Consequently, the corresponding error rotation vector is the reverse of that for the RIEKF. In addition, the filter in [32] estimates the angular velocity using star sensor measurements directly instead of using gyroscopes,

Table 1: Monte Carlo simulation parameters

	Section VI.A	Section VI.B	Section VI.C
covariance of Sun sensor noise $\boldsymbol{v}^1$, rad	$0.0017^2\boldsymbol{I}_3$	$0.0175^2\boldsymbol{I}_3$	$0.0175^2\boldsymbol{I}_3$
covariance of magnetometer noise $\boldsymbol{v}^2$, rad	$0.0087^2\boldsymbol{I}_3$	$0.0873^2\boldsymbol{I}_3$	$0.0873^2\boldsymbol{I}_3$
standard deviation of bias noise σ_v, rad/s$^{3/2}$	$\sqrt{10}\times10^{-7}$	$\sqrt{10}\times10^{-7}$	$\sqrt{10}\times10^{-5}$
standard deviation of gyro noise σ_u, rad/s$^{3/2}$	$\sqrt{10}\times10^{-10}$	$\sqrt{10}\times10^{-10}$	$\sqrt{10}\times10^{-8}$
initial attitude estimate $\hat{\boldsymbol{q}}(0)$	$\mathbf{1}$	$\mathbf{1}$	$\mathbf{1}$
initial bias estimate $\hat{\boldsymbol{\beta}}(0)$, rad/s	$[0,0,0]^T$	$[0,0,0]^T$	$[0,0,0]^T$
initial covariance for attitude error, deg^2	$10^2\boldsymbol{I}_3$	$150^2\boldsymbol{I}_3$	$10^2\boldsymbol{I}_3$
initial covariance for bias error, (deg/h)^2	$3^2\boldsymbol{I}_3$	$20^2\boldsymbol{I}_3$	$5^2\boldsymbol{I}_3$
vector measurement frequency, Hz	1	1	1
gyro measurement frequency, Hz	0.1	0.1	0.1
running time span, min	35	65	85
total number of simulations	100	100	100

and the angular velocity estimation error are defined in the spacecraft body frame rather than the inertial frame.

VI. Numerical Examples

In this section, the proposed quaternion RIEKF and LIEKF are examined via simulated spacecraft attitude determination examples. Their performance is compared with the quaternion MEKF [31] and the CKF developed in [16]. In particular, the simulations also include the MEKF and LIEKF incorporating the covariance resetting algorithm developed in [21], which are termed covariance-reset MEKF (CRMEKF) and LIEKF (CRLIEKF) respectively. Three sets of Monte Carlo simulations are conducted respectively for three scenarios with small initial estimation errors, large initial estimation errors, and a severe initial condition where the initial error covariance is chosen small while the initial state error is extremely large.

Consider a rigid spacecraft that is freely tumbling in a circular orbit with an altitude of 500 km, an inclination angle of 60 deg, a right ascension of the ascending node of 120 deg, an argument perigee

of 0 deg, and an initial true anomaly 0 deg at the epoch 12:00 UTC, 1 June 2015. The spacecraft has an inertia of $\boldsymbol{J} = \text{diag}\{60, 53, 70\}$ kg/m^2. The spacecraft angular velocity is governed by the Euler dynamics $\boldsymbol{J}\dot{\boldsymbol{\omega}} + \boldsymbol{\omega} \times \boldsymbol{J}\boldsymbol{\omega} = \boldsymbol{\tau}_g$ with the initial angular velocity $\boldsymbol{\omega}(0) = [0.02, -0.04, -0.02]$ rad/s. $\boldsymbol{\tau}_g = 3\mu \boldsymbol{r}_{sc} \times \boldsymbol{J}\boldsymbol{r}_{sc}/\|\boldsymbol{r}_{sc}\|^5$ is the Earth's gravity gradient torque, where $\mu = 398,600.4418\,\text{kg}^3/\text{s}^2$ is the Earth's gravitational parameter and $\boldsymbol{r}_{sc}$ is the spacecraft position vector relative to the Earth center expressed in the spacecraft body frame.

It is assumed that the spacecraft is equipped with sun sensors, which measure the sun vector at 1 Hz sampling frequency, and magnetometers, which measures the Earth's magnetic field at the same sampling frequency. Let $\boldsymbol{r}^1$ be the sun vector and $\boldsymbol{r}^2$ the unit magnetic-field vector. Accordingly, $\boldsymbol{v}^1$ and $\boldsymbol{v}^2$ are the zero-mean white sensor noise associated with the vector measurements. The three-axis rate gyros measure the spacecraft angular velocity at a frequency of 0.1 Hz. The sun vector is assumed to be inertially constant for the duration of the simulation. The magnetic field vector is obtained from the IGRF-12 model [33].

In order to evaluate the estimation accuracy, the following root mean squared errors (RMSE) are defined:

$$\|\tilde{\boldsymbol{\gamma}}\|_{\text{RMSE}} = \sqrt{\tfrac{1}{M}\sum_{j=1}^{M} \|\tilde{\boldsymbol{\gamma}}^j\|^2}$$
$$\|\Delta\boldsymbol{\beta}\|_{\text{RMSE}} = \sqrt{\tfrac{1}{M}\sum_{j=1}^{M} \|\Delta\boldsymbol{\beta}^j\|^2}, \quad \Delta\boldsymbol{\beta}^j = \hat{\boldsymbol{\beta}}^j - \boldsymbol{\beta}^j$$

where $\tilde{\boldsymbol{\gamma}}^j$ and $\Delta\boldsymbol{\beta}^j$ are respectively the error principal rotation vector and bias estimation error vector for the j-th Monte Carlo run, $j = 1, \cdots, M$. Clearly, $\|\tilde{\boldsymbol{\gamma}}\|_{\text{RMSE}}$ and $\|\Delta\boldsymbol{\beta}\|_{\text{RMSE}}$ measure the average estimation error for the spacecraft attitude and gyro bias in M-times simulations respectively. It does not matter that $\tilde{\boldsymbol{\gamma}}^j$ denotes the attitude error of the RIEKF or the LIEKF because, as mentioned in Section V, the attitude errors of these two filters are related to each other by means of a coordinate transformation which preserves their Euclidean norms.

A. Simulations with Small Initial Estimation Errors

The first set of simulations runs 100 times and compares the performance of the MEKF, CKF, LIEKF, RIEKF, CRMEKF, and CRLIEKF for the case of small initial estimation errors. The initial attitude estimate and bias estimate are all fixed to $\hat{\boldsymbol{q}}(0) = \boldsymbol{1}$ and $\hat{\boldsymbol{\beta}}(0) = [0, 0, 0]^T$ rad/s. For all four

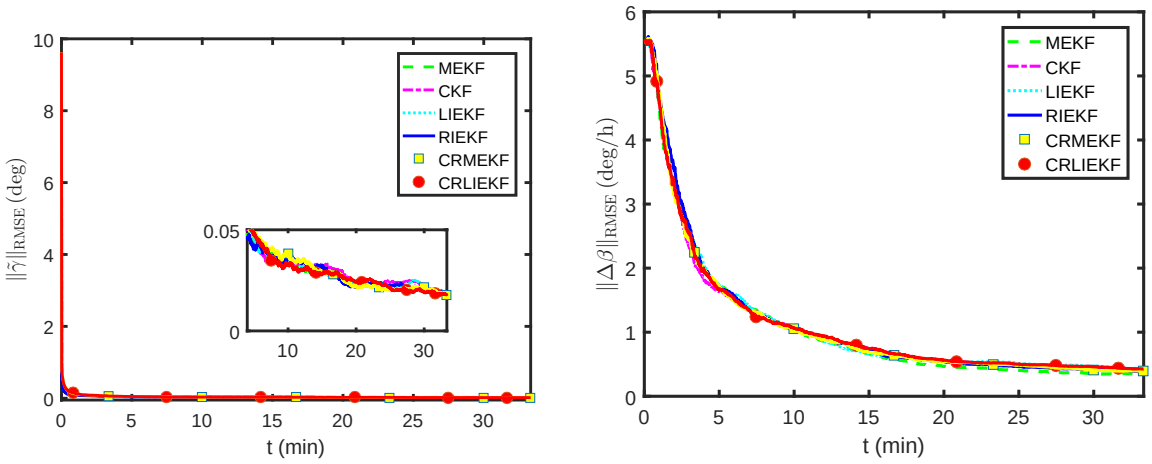

(a) (b)

Fig. 1: RMSE of $\|\tilde{\boldsymbol{\gamma}}\|$ and $\|\Delta\boldsymbol{\beta}\|$ for small initial estimation errors

methods, the true initial attitude $\boldsymbol{q}(0) = (\exp_q(\tilde{\boldsymbol{\gamma}}(0)/2))^* \otimes \hat{\boldsymbol{q}}(0)$ and gyro bias $\boldsymbol{\beta}(0)$ are randomly generated such that $\tilde{\boldsymbol{\gamma}}(0)$ follows the normal distribution $\mathcal{N}(0, (10\,\mathrm{deg})^2\boldsymbol{I}_3)$ and $\Delta\boldsymbol{\beta}(0) = \hat{\boldsymbol{\beta}}(0) - \boldsymbol{\beta}(0)$ follows the normal distribution $\mathcal{N}(0, (3\,\mathrm{deg/h})^2\boldsymbol{I}_3)$, respectively. Hence, the initial covariance for the RIEKF is given by $\boldsymbol{P}_{\mathrm{RIEKF}}(0) = \mathrm{diag}\{0.1745^2\boldsymbol{I}_3, (1.4544\times10^{-5})^2\boldsymbol{I}_3\}$. According to Eq. (40), the initial covariances for the MEKF, LIEKF, CRMEKF, and CRLIEKF are the same as $\boldsymbol{P}_{\mathrm{RIEKF}}(0)$. The initial covariance for the CKF is set to $\boldsymbol{P}_{\mathrm{CKF}}(0) = \mathrm{diag}\{0.01^2, 0.0873^2\boldsymbol{I}_3, (1.4544\times10^{-5})^2\boldsymbol{I}_3\}$.

Table 1 summarizes other simulation parameters. As shown in Table 1, the standard deviation of the sun sensor noise is 0.0017 rad, which approximates to a deviation angle of 0.1 deg, and the standard deviation of the magnetometer noise is 0.0087 rad, which approximates to a deviation angle of 0.5 deg. The standard deviations of the two gyro noise parameters are $\sigma_v = \sqrt{10}\times10^{-10}$ rad/s$^{3/2}$ and $\sigma_u = \sqrt{10}\times10^{-7}$ rad/s$^{3/2}$. The simulation time spans 35 minutes.

The simulation results are displayed in Figs. 1-3. Figure 1 compares the average attitude error and bias error for all four methods, which provide nearly indistinguishable performances from each other in the considered scenario. In the steady phase, the RMSE of the attitude estimate is about 0.02 deg and that of the bias estimate is about 0.3 deg/h.

Figures 2 and 3 show the 100 instances of the attitude error and the bias error in the first axis (i.e., $\tilde{\gamma}_1$ and $\Delta\beta_1$) respectively for each method. For clarity, we also include the zoomed local

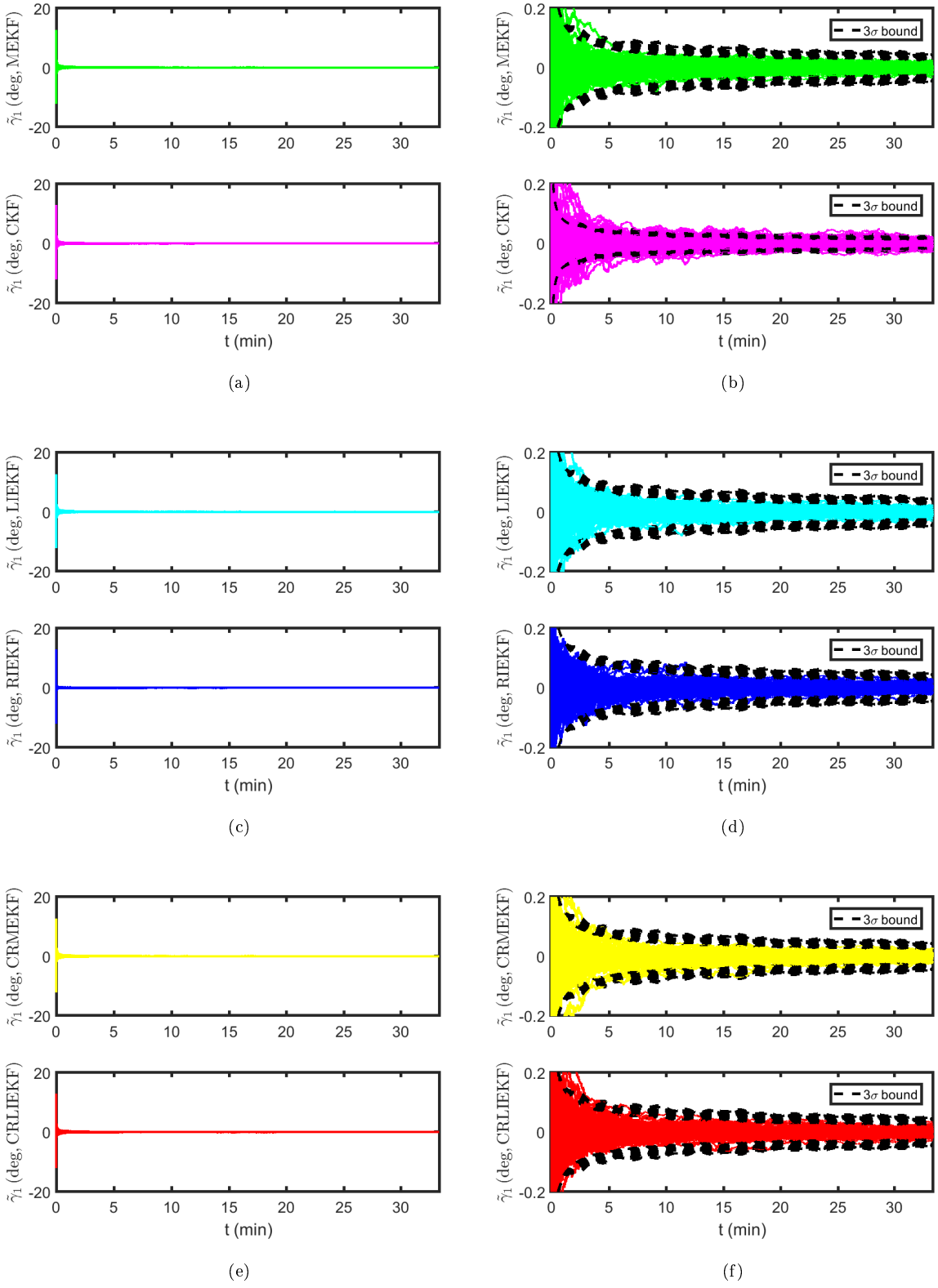

Fig. 2: Attitude estimation error $\tilde{\gamma}_1$ for all filters with small initial estimation errors

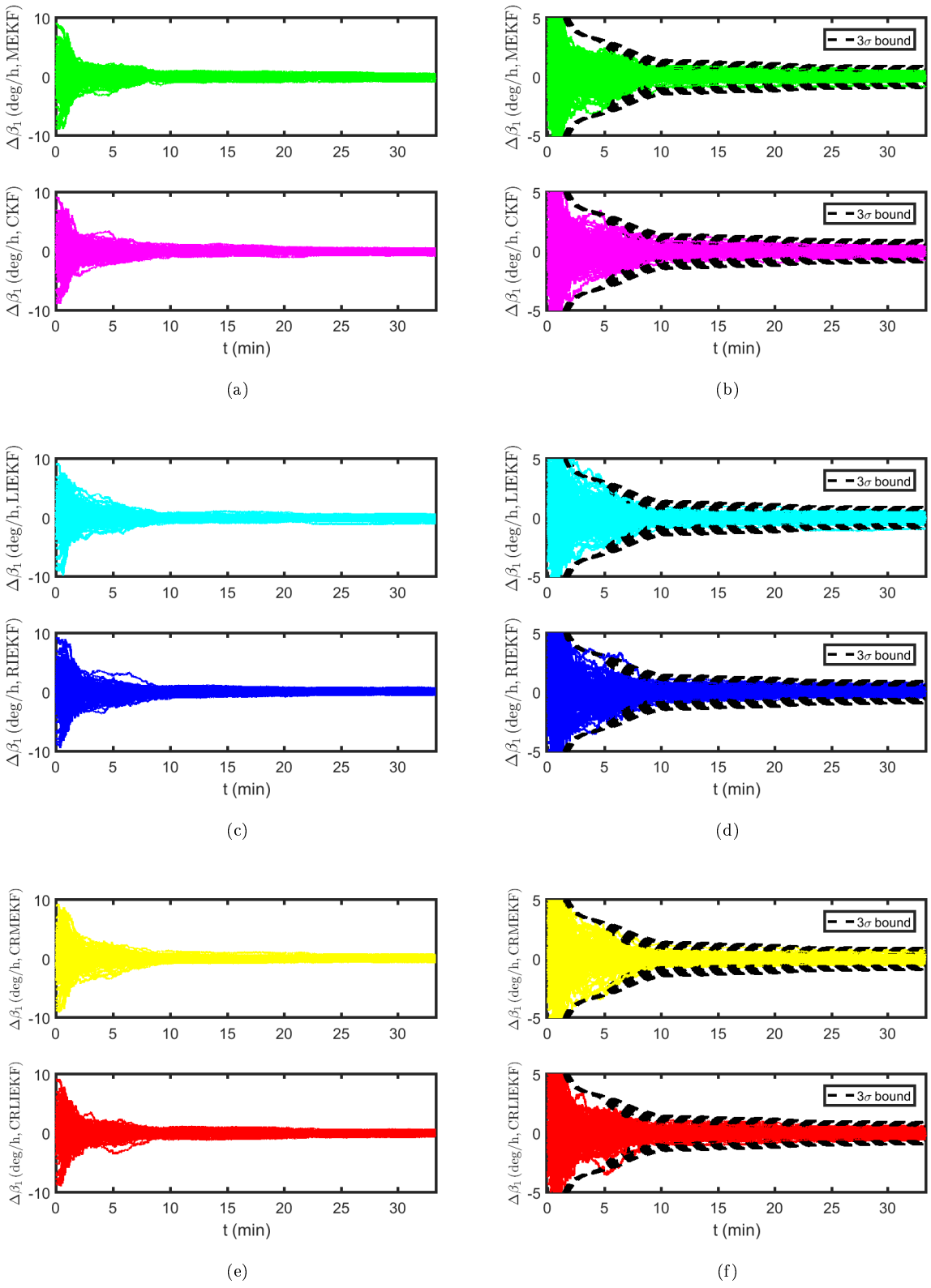

Fig. 3: Gyro bias estimation error $\Delta\boldsymbol{\beta}_1$ for all filters with small initial estimation errors

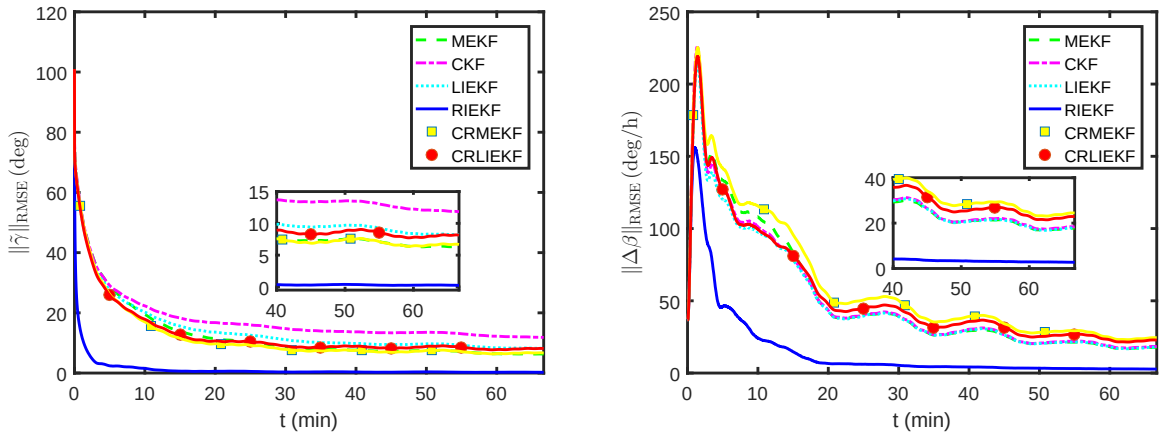

Fig. 4: RMSE of $\|\tilde{\boldsymbol{\gamma}}\|$ and $\|\Delta\boldsymbol{\beta}\|$ for large initial estimation errors

views for $\tilde{\gamma}_1 \in [0.2, -0.2]$ deg and $\Delta\beta_1 \in [-5, 5]$ with 100 instances of 3σ bounds predicted by the estimation error covariances. As can be seen, the behavior of the MEKF, LIEKF, CRMEKF, and CRLIEKF is almost identical. The RIEKF predicts slightly better 3σ bounds on the attitude error than the other filters, especially during the time interval $[0, 3]$ min. In the steady phase, the CKF slightly underestimates the attitude error covariance while the other filters capture the estimation uncertainty satisfactorily and there is no significant difference among them (Fig. 3).

B. Simulations with Large Initial Estimation Errors

The second set of simulations investigates a different scenario when the initial estimation error is considerably large. Most of the simulation parameters are given in Table 1. As can be seen, the initial attitude estimate and bias estimate are all fixed and remain the same. The initial attitude error covariance is $(150\,\mathrm{deg})^2$ in each axis and the initial bias error covariance is $(20\,\mathrm{deg/h})^2$ in each axis. Consequently, the initial covariances for the RIEKF, MEKF, LIEKF, CRMEKF, and CRLIEKF are computed as $\mathrm{diag}\{2.618^2\boldsymbol{I}_3, (9.6963\times10^{-5})^2\boldsymbol{I}_3\}$ while that for the CKF is given by $\boldsymbol{P}_{\mathrm{CKF}}(0) = \mathrm{diag}\{0.01^2, 1.309^2\boldsymbol{I}_3, (9.6963\times10^{-5})^2\boldsymbol{I}_3\}$. The true initial attitude and gyro bias are then generated randomly such that $\tilde{\boldsymbol{\gamma}}(0) \sim \mathcal{N}(0, (150\,\mathrm{deg})^2\boldsymbol{I}_3)$ and $\Delta\boldsymbol{\beta}(0) \sim \mathcal{N}(0, (20\,\mathrm{deg/h})^2\boldsymbol{I}_3)$. In addition, the standard deviation for the sun vector measurement noise is increased to 0.0175 rad

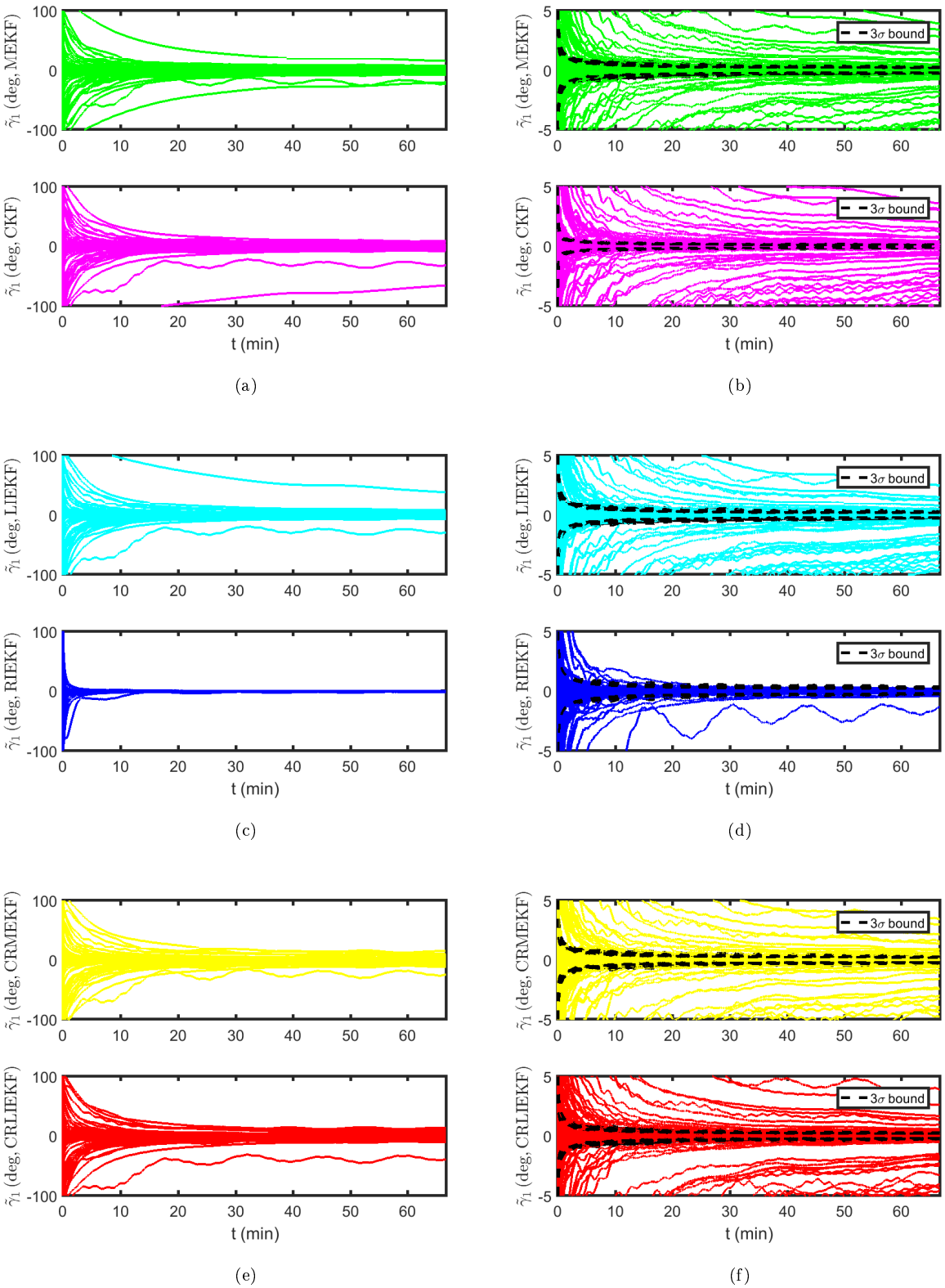

Fig. 5: Attitude estimation error $\tilde{\gamma}_1$ for all filters with large initial estimation errors

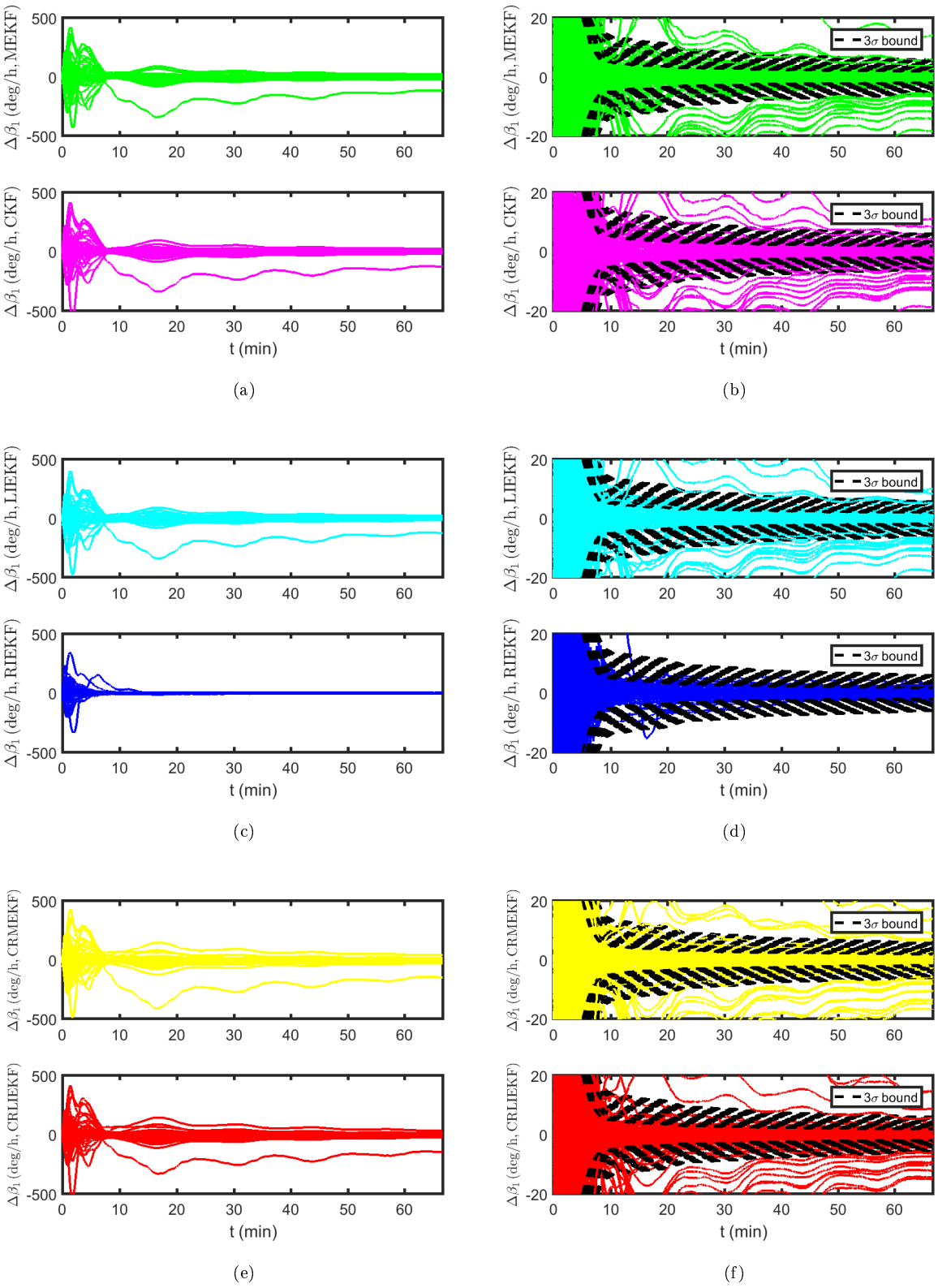

Fig. 6: Gyro bias estimation error $\Delta\boldsymbol{\beta}_1$ for all filters with large initial estimation errors

($\approx 1\,\text{deg}$) while that for the unit magnetic-field vector is 0.0873 rad ($\approx 5\,\text{deg}$). The simulation spans 65 min.

A total of 100 simulations are conducted for each of the six filters. The results are plotted in Figs. 4-6, which show the RMSE of attitude estimates and gyro bias estimates and the 100 instances of the attitude error $\tilde{\gamma}_1$ and bias error $\Delta\beta_1$ respectively. In this severe case, all filters do provide convergent estimations but the respective convergence speed and estimation accuracy are different. The CRMEKF and CRLIEKF provide slightly smaller attitude estimation errors and slightly larger bias estimation errors than the MEKF and LIEKF. This is probably because the noise processes applied are isotropic and the attitude covariances are approximately diagonal with almost equal eigenvalues. As a result, the covariance mapping has little effect [21]. It can also be seen that the RIEKF demonstrates significantly better performance than the other five filters. More precisely, the RIEKF takes 10 min to decrease $\|\tilde{\boldsymbol{\gamma}}\|_{\text{RMSE}}$ below 2 deg, and 20 min to decrease $\|\Delta\boldsymbol{\beta}\|_{\text{RMSE}}$ below 8.5 deg/h. The average attitude error and bias error in steady phase are about 0.37 deg and 2.8 deg/h respectively. In contrast, the other filters never achieve estimation accuracy comparable to the RIEKF in the entire simulation time span. The steady-state RMSE of attitude is about 15 deg for the CKF, 8.5 deg for the MEKF and LIEKF, and 6.5 deg for the CRMEKF and CRLIEKF while the steady-state RMSE of gyro bias for the MEKF, LIEKF, and CKF is about 17.5 deg/h, and for the CRMEKF and CRLIEKF is about 23 deg/h. Therefore, the RIEKF not only achieves faster convergence but also higher estimation accuracy.

As shown in Figs. 5 and 6, the RIEKF provides more concentrated estimation trajectories and hence its performance is less sensitive to the initial errors than the other filters. Moreover, the 3σ bounds of the RIEKF capture most of the error dispersion while many of the 100 instances stay outside the 3σ bounds of the other filters. Hence, the RIEKF provides better indication of the level of estimation uncertainty. Additionally, the difference between MEKF and LIEKF is also invisible in this case.

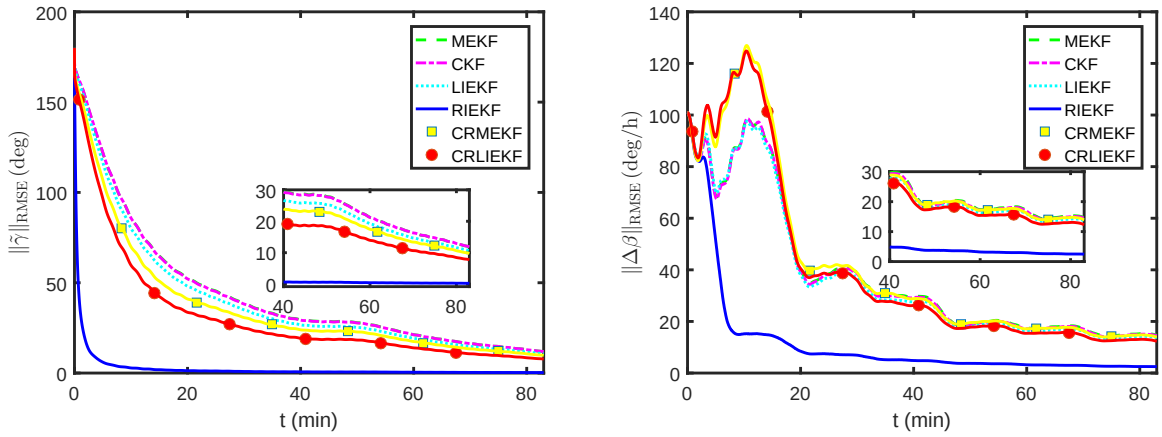

(a) (b)

Fig. 7: RMSE of $\|\tilde{\boldsymbol{\gamma}}\|$ and $\|\Delta\boldsymbol{\beta}\|$ for a severe initial condition

C. Simulations with a Severe Initial Condition

This section considers a severe case that the initial attitude and bias errors are very large while all filters are given a small yet erroneous initial error covariance. The simulation parameters can be found in Table 1. For all filters, the standard deviation of the initial attitude error in each axis is 10 deg and that of the bias error is 5 deg/h. This implies that the initial covariances for implementing the RIEKF, MEKF, LIEKF, CRMEKF, and CRLIEKF are set to $\mathrm{diag}\{0.1745^2\boldsymbol{I}_3, (2.4241\times 10^{-5})^2\boldsymbol{I}_3\}$ and that for the CKF is given by $\boldsymbol{P}_{\mathrm{CKF}}(0) = \mathrm{diag}\{0.01^2, 0.0873^2\boldsymbol{I}_3, (2.4241\times 10^{-5})^2\boldsymbol{I}_3\}$. The initial estimates remain to be $\hat{\boldsymbol{q}} = \mathbf{1}$ and $\hat{\boldsymbol{\beta}}(0) = [0,0,0]^T$ rad/s while the true initial attitude and gyro bias are set to $\boldsymbol{q}(0) = [0,1,0,0]^T$ and $\boldsymbol{\beta}(0) = [100,10,10]$ deg/h. In other words, the estimated attitude is 180 deg from the true attitude and the estimated gyro bias in the first axis is far smaller than the true bias. Therefore, the chosen initial covariance gives incorrect indication of the initial estimation error. The noise magnitude associated with the vector measurements remains the same as Section VI.B. The standard deviations of the two gyro noise processes $\boldsymbol{\eta}_v$ and $\boldsymbol{\eta}_u$ are increased to $\sqrt{10}\times 10^{-8}$ rad/s$^{3/2}$ and $\sqrt{10}\times 10^{-5}$ rad/s$^{3/2}$. The simulation spans 85 min.

Figures 7-9 plot the results for 100 simulation runs, showing the average attitude error and bias error, the attitude estimation error $\tilde{\gamma}_1$, and the bias estimation error $\Delta\beta_1$. Compared to the MEKF and LIEKF, the CRMEKF and CRLIEKF both improves the estimation accuracy of the

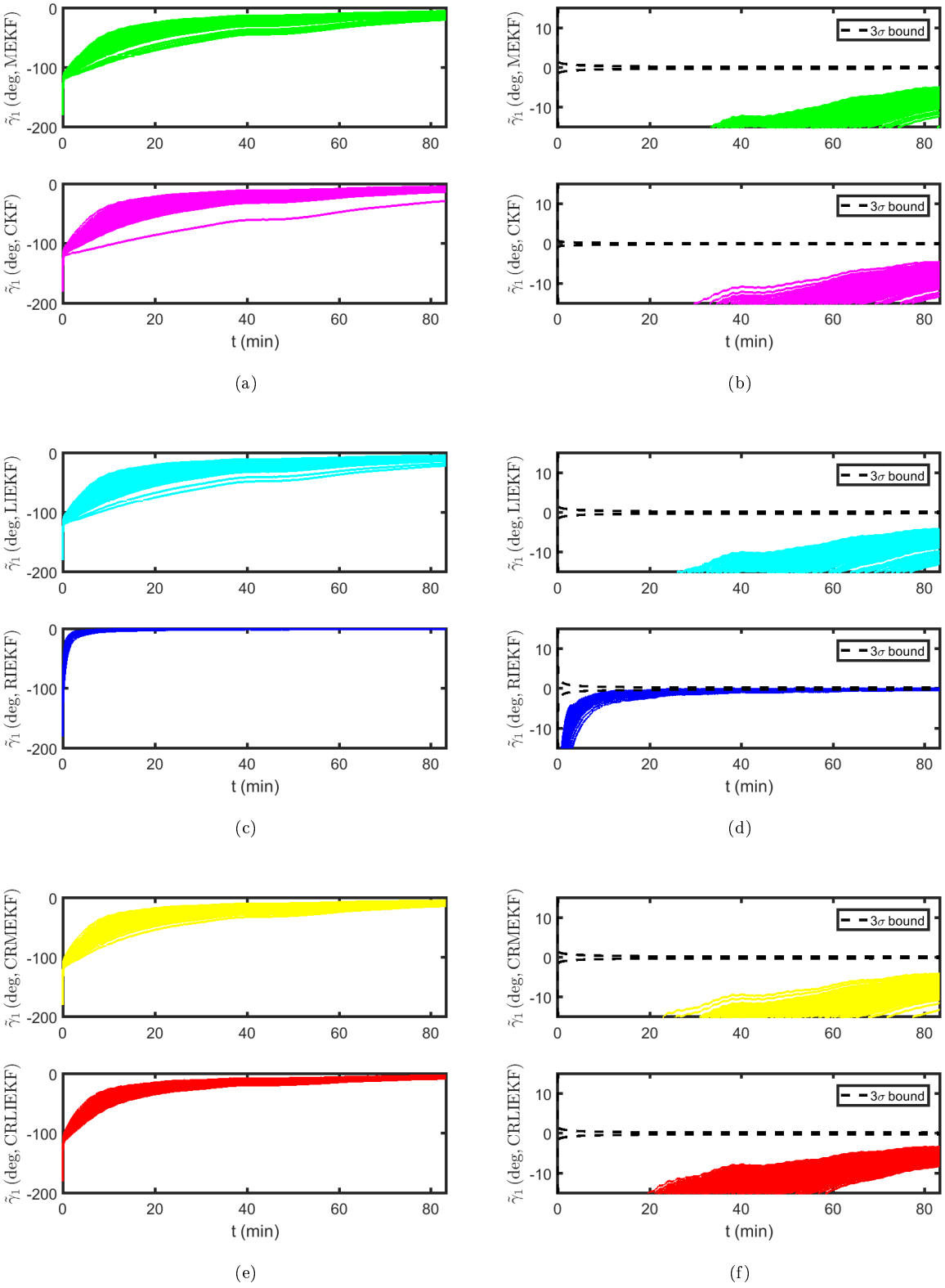

Fig. 8: Attitude estimation error $\tilde{\gamma}_1$ for all filters with a severe initial condition

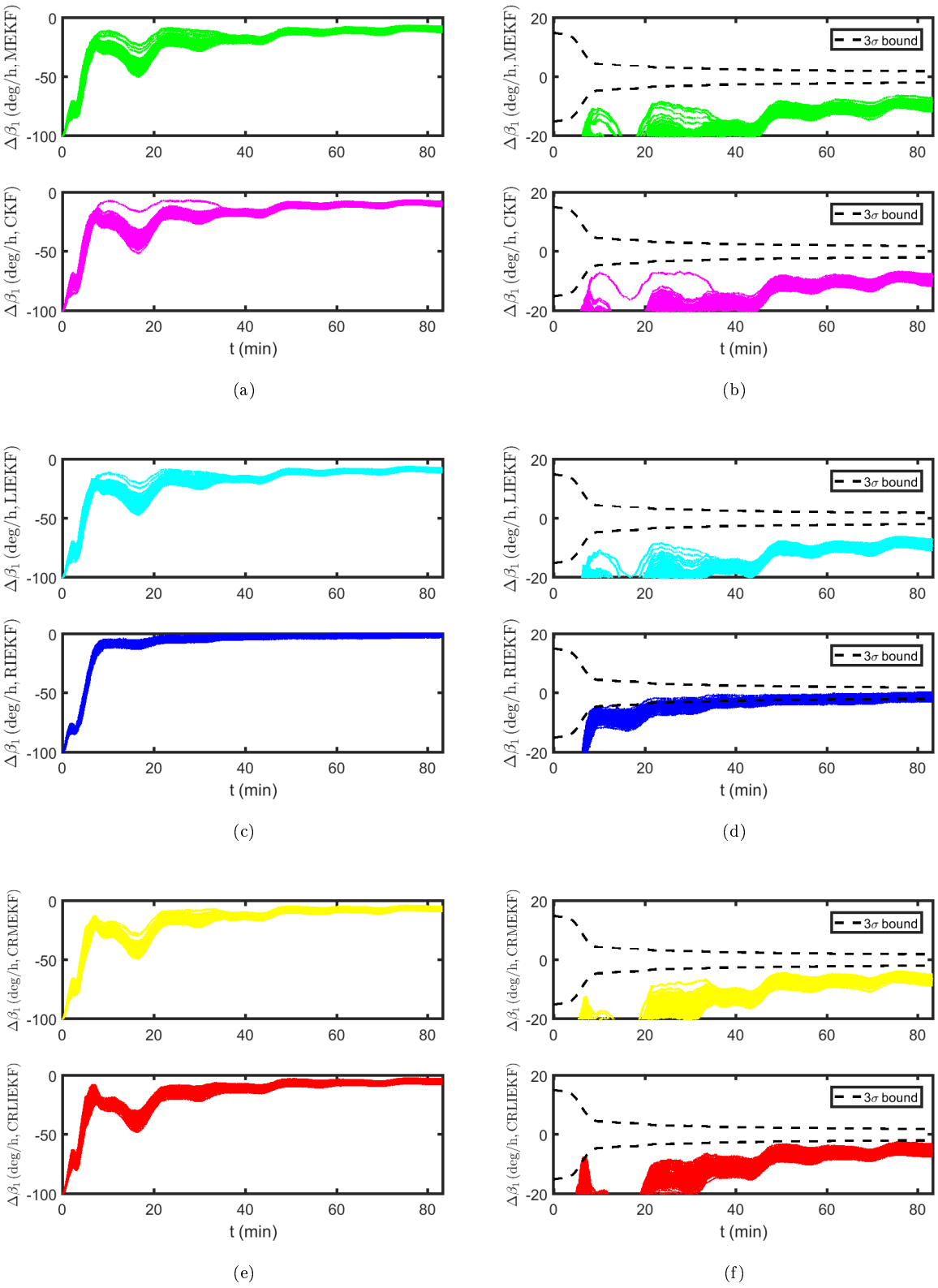

Fig. 9: Gyro bias estimation error $\Delta\boldsymbol{\beta}_1$ for all filters with a severe initial condition

attitude estimate and gyro bias estimate in this scenario. In addition, the peak bias error in Fig. 7b is less than that in Fig. 4b, even though the initial bias error is much higher here. This is mainly due to the small initial error covariance applied here, which tends to produce small corrections and lower transient overshoots. It can also be seen that the RIEKF attains better performance than the other filters, in terms of convergence speed, steady-state estimation accuracy, and prediction of the estimation uncertainty. The behaviors of the MEKF, CKF, and LIEKF are similar to each other and at the end of the simulation their steady-state RMSE for the attitude error is about 12 deg, and for the bias error is about 15 deg/h. For the CRMEKF and CRLIEKF, the steady-state RMSE of the attitude error is about 10 deg and 8 deg respectively, and of the bias error is about 13.8 deg/h and 12 deg/h respectively. In contrast, the RIEKF achieves an average attitude error of 0.8 deg in 20 min, and an average bias error of 3 deg/h in 60 min.

As shown in Figs. 8 and 9, the RIEKF again produces more concentrated estimation trajectories than the other filters. The MEKF, CKF, LIEKF, CRMEKF, and CRLIEKF all fail to capture the error dispersion in the attitude estimate and bias estimate for all 100 instances. For the RIEKF, the estimation error trajectories stay outside the predicted 3σ envelope but in the steady phase many of them gradually enter the envelope.

VII. Conclusion

Two continuous-discrete quaternion invariant extended Kalman filters (IEKFs) were developed via the invariant Kalman filter theory, namely, the right IEKF (RIEKF) and the left IEKF (LIEKF). They both respect the unit-norm constraint of unit quaternions by utilizing the quaternion exponential map for corrections but build on two different types of output-state errors, which are constructed from two different invariance properties of the system dynamics. The LIEKF is almost identical to the classical quaternion MEKF except the correction step. From the perspective of invariant Kalman filter theory the quaternion MEKF is actually a LIEKF employing corrections within first-order approximation. Compared to the LIEKF and MEKF, the RIEKF depends less on the estimated trajectory since its sensitivity matrix and attitude estimation error equation are both independent of the estimated states, and therefore achieves better robustness. Monte Carlo

simulations were conducted to compare the performance of the proposed invariant filters with the MEKF, the unit-norm constrained Kalman filter (CKF), and two filters improved with the covariance mapping. The results have shown that the RIEKF and LIEKF provide similar performance to the compared filters when the initial estimation error is small. In some severe scenarios such as large initial estimation errors or erroneous initial error covariances, the RIEKF demonstrates faster convergence, more accurate estimation, and better prediction of the estimation uncertainty than the other methods.

Appendix: Derivation of Eqs. (24) and (25)

Derivation of Eq. (24): Differentiating $\tilde{\boldsymbol{q}}$ defined in Eq. (14) and invoking Eqs. (5), (6) and (15), one can derive

$$\begin{aligned}\dot{\tilde{\boldsymbol{q}}} &= \dot{\hat{\boldsymbol{q}}} \otimes \boldsymbol{q}^* + \hat{\boldsymbol{q}} \otimes \dot{\boldsymbol{q}}^* \\ &= \tfrac{1}{2}\hat{\boldsymbol{q}} \otimes (\bar{\boldsymbol{\omega}} - \hat{\boldsymbol{\beta}}) \otimes \boldsymbol{q}^* - \tfrac{1}{2}\hat{\boldsymbol{q}} \otimes (\bar{\boldsymbol{\omega}} - \boldsymbol{\beta} - \boldsymbol{\eta}_v) \otimes \boldsymbol{q}^* \\ &= -\tfrac{1}{2}\hat{\boldsymbol{q}} \otimes (\hat{\boldsymbol{\beta}} - \boldsymbol{\beta}) \otimes \boldsymbol{q}^* + \tfrac{1}{2}\hat{\boldsymbol{q}} \otimes \boldsymbol{\eta}_v \otimes \boldsymbol{q}^*\end{aligned}$$

Invoking $\hat{\boldsymbol{q}} = \tilde{\boldsymbol{q}} \otimes \boldsymbol{q}$ and $\boldsymbol{q}^* = \hat{\boldsymbol{q}}^* \otimes \tilde{\boldsymbol{q}}$ and letting $\hat{\boldsymbol{\eta}}_v = \hat{\boldsymbol{q}} \otimes \boldsymbol{\eta}_v \otimes \hat{\boldsymbol{q}}^*$ leads to

$$\begin{aligned}\dot{\tilde{\boldsymbol{q}}} &= -\tfrac{1}{2}\tilde{\boldsymbol{q}} \otimes \boldsymbol{q} \otimes (\hat{\boldsymbol{\beta}} - \boldsymbol{\beta}) \otimes \boldsymbol{q}^* + \tfrac{1}{2}\hat{\boldsymbol{q}} \otimes \boldsymbol{\eta}_v \otimes \hat{\boldsymbol{q}}^* \otimes \tilde{\boldsymbol{q}} \\ &= -\tfrac{1}{2}\tilde{\boldsymbol{q}} \otimes \tilde{\boldsymbol{\beta}} + \tfrac{1}{2}\hat{\boldsymbol{\eta}}_v \otimes \tilde{\boldsymbol{q}}\end{aligned}$$

which is exactly Eq. (24).

Derivation of Eq. (25): Similarly, differentiating $\tilde{\boldsymbol{\beta}}$ defined in Eq. (14) and invoking Eqs. (5)-(7) and (15) yields

$$\begin{aligned}\dot{\tilde{\boldsymbol{\beta}}} &= \dot{\boldsymbol{q}} \otimes (\hat{\boldsymbol{\beta}} - \boldsymbol{\beta}) \otimes \boldsymbol{q}^* + \boldsymbol{q} \otimes (\hat{\boldsymbol{\beta}} - \boldsymbol{\beta}) \otimes \dot{\boldsymbol{q}}^* - \boldsymbol{q} \otimes \dot{\boldsymbol{\beta}} \times \boldsymbol{q}^* \\ &= \tfrac{1}{2}\boldsymbol{q} \otimes (\bar{\boldsymbol{\omega}} - \boldsymbol{\beta} - \boldsymbol{\eta}_v) \otimes (\hat{\boldsymbol{\beta}} - \boldsymbol{\beta}) \otimes \boldsymbol{q}^* \\ &\quad -\tfrac{1}{2}\boldsymbol{q} \otimes (\hat{\boldsymbol{\beta}} - \boldsymbol{\beta}) \otimes (\bar{\boldsymbol{\omega}} - \boldsymbol{\beta} - \boldsymbol{\eta}_u) \otimes \boldsymbol{q}^* - \boldsymbol{q} \otimes \boldsymbol{\eta}_u \otimes \boldsymbol{q}^* \\ &= \boldsymbol{q} \otimes [(\bar{\boldsymbol{\omega}} - \boldsymbol{\beta} - \boldsymbol{\eta}_u) \times (\hat{\boldsymbol{\beta}} - \boldsymbol{\beta}) - \boldsymbol{\eta}_u] \otimes \boldsymbol{q}^*\end{aligned}$$

Noting that $\bar{\boldsymbol{\omega}} - \boldsymbol{\beta} = \bar{\boldsymbol{\omega}} - \hat{\boldsymbol{\beta}} + \hat{\boldsymbol{\beta}} - \boldsymbol{\beta}$, $(\hat{\boldsymbol{\beta}} - \boldsymbol{\beta}) \times (\hat{\boldsymbol{\beta}} - \boldsymbol{\beta}) = 0$ and $\boldsymbol{q} = \tilde{\boldsymbol{q}}^* \otimes \hat{\boldsymbol{q}}$, one can further derive

$$
\begin{aligned}
\dot{\tilde{\boldsymbol{\beta}}} &= \boldsymbol{q} \otimes [(\bar{\boldsymbol{\omega}} - \hat{\boldsymbol{\beta}} - \boldsymbol{\eta}_u) \times (\hat{\boldsymbol{\beta}} - \boldsymbol{\beta}) - \boldsymbol{\eta}_u] \otimes \boldsymbol{q}^* \\
&= [\boldsymbol{q} \otimes (\bar{\boldsymbol{\omega}} - \hat{\boldsymbol{\beta}} - \boldsymbol{\eta}_u) \otimes \boldsymbol{q}^*] \times \tilde{\boldsymbol{\beta}} - \boldsymbol{q} \otimes \boldsymbol{\eta}_u \otimes \boldsymbol{q}^* \\
&= [\tilde{\boldsymbol{q}}^* \otimes (\hat{\boldsymbol{I}}_\omega - \hat{\boldsymbol{\eta}}_u) \otimes \tilde{\boldsymbol{q}}] \times \tilde{\boldsymbol{\beta}} - \tilde{\boldsymbol{q}}^* \otimes \hat{\boldsymbol{\eta}}_u \otimes \tilde{\boldsymbol{q}}
\end{aligned}
$$

Recalling $\tilde{\boldsymbol{q}}^* \otimes \boldsymbol{x} \otimes \tilde{\boldsymbol{q}} = \boldsymbol{A}(\tilde{\boldsymbol{q}})\boldsymbol{x}$ for any $\boldsymbol{x} \in \mathbb{R}^3$ arrives at Eq. (25).

Acknowledgments

The authors would like to thank the associate editor and the anonymous reviewer for all the insightful comments that led to significant improvement of the paper. The work of the first author in this paper has received funding from the National Natural Science Foundation of China (11702010).

References

[1] Black, H. D., "A Passive System for Determining the Attitude of a Satellite," *AIAA Journal*, Vol. 2, No. 7, 1964, pp. 1350–1351,
doi:10.2514/3.2555.

[2] Bar-Itzhack, I. Y. and Reiner, J., "Recursive Attitude Determination from Vector Observations: Direction Cosine Matrix Identification," *AIAA Journal of Guidance, Control, and Dynamics*, Vol. 7, No. 1, 1984, pp. 151–56,
doi:10.2514/3.56362.

[3] Shuster, M. D. and Oh, S. D., "Three-Axis Attitude Determination from Vector Observations," *AIAA Journal of Guidance, Control, and Dynamics*, Vol. 4, No. 1, 1981, pp. 70–77,
doi:10.2514/3.19717.

[4] Bar-Itzhack, I. Y., "REQUEST: A Recursive QUEST Algorithm for Sequential Attitude Determination," *AIAA Journal of Guidance, Control, and Dynamics*, Vol. 19, No. 5, 1996, pp. 1034–1038,
doi:10.2514/3.21742.

[5] Mortari, D., "ESOQ: A Closed-Form Solution to the Wahba Problem," *Journal of the Astronautical Sceinces*, Vol. 45, No. 2, 1997, pp. 195–204.

[6] Lefferts, E. J., Markley, F. L., and Shuster, M. D., "Kalman Filtering for Spacecraft Attitude Estimation," *AIAA Journal of Guidance, Control, and Dynamics*, Vol. 5, No. 5, 1982, pp. 417–429,
doi:10.2514/3.56190.

[7] Psiaki, M. L. and Oshman, Y., "Three-Axis Attitude Determination via Kalman Filtering of Magnetometer Data," *AIAA Journal of Guidance, Control, and Dynamics*, Vol. 13, No. 3, 1990, pp. 506–514, doi:10.2514/3.25364.

[8] Crassidis, J. L. and Markley, F. L., "Attitude Estimation Using Modified Rodrigues Parameters," *Proceedings of the Flight Mechanics/ Estimation Theory Symposium*, pp. 71–83. NASA Goddard Space Flight Center, Greenbelt, MD, 1996.

[9] de Ruiter, A. H. J., Tran, L., Kumar, B. S., and Muntyanov, A., "Sun Vector-Based Attitude Determination of Passively Magnetically Stabilized Spacecraft," *AIAA Journal of Guidance, Control and Dynamics*, Vol. 39, No. 7, 2016, pp. 1551–1562, doi:10.2514/1.G001757.

[10] Mahony, R., Hamel, T., and Pflimlin, J.-M., "Nonlinear Complementary Filters on the Special Orthogonal Group," *IEEE Transactions on Automatic Control*, Vol. 53, No. 5, 2008, pp. 1203–1218, doi:10.1109/TAC.2008.923738.

[11] Izadi, M. and Sanyal, A. K., "Rigid Body Attitude Estimation Based on the Lagrange-d'Alembert Principle," *Automatica*, Vol. 50, No. 10, 2014, pp. 2570–2577, doi:10.1016/j.automatica.2014.08.010.

[12] Zlotnik, D. E. and Forbes, J. R., "Nonlinear Estimator Design on the Special Orthogonal Group Using Vector Measurements Directly," *IEEE Transactions on Automatic Control*, Vol. 62, No. 1, 2017, pp. 149–160, doi:10.1109/TAC.2016.2547222.

[13] Crassidis, J. L., Markley, F. L., and Cheng, Y., "Survey of Nonlinear Attitude Estimation Methods," *AIAA Journal of Guidance, Control, and Dynamics*, Vol. 30, No. 1, 2007, pp. 12–28, doi:10.2514/1.22452.

[14] de Ruiter, A. H. J. and Forbes, J. R., "Discrete-Time SO(n)-Constrained Kalman Filtering," *AIAA Journal of Guidance, Control and Dynamics*, Vol. 40, No. 1, 2017, pp. 28–37, doi:10.2514/1.G001653.

[15] Markley, F. L., "Attitude Error Representations for Kalman Filtering," *Journal of Guidance, Control, and Dynamics*, Vol. 63, No. 2, 2003, pp. 311–317, doi:10.2514/2.5048.

[16] Zanetti, R., Majji, M., Bishop, R. H., and Mortari, D., "Norm-Constrained Kalman Filtering," *AIAA Journal of Guidance, Control, and Dynamics*, Vol. 32, No. 5, 2009, pp. 1458–1465, doi:10.2514/1.43119.

[17] Forbes, J. R., de Ruiter, A. H. J., and Zlotnik, D. E., "Continuous-Time Norm-Constrained Kalman Filtering," *Automatica*, Vol. 50, 2014, pp. 2546–2554, doi:10.1016/j.automatica.2014.08.007.

[18] Psiaki, M. L., "Attitude-Determination Filtering via Extended Quaternion Estimation," *AIAA Journal of Guidance, Control, and Dynamics*, Vol. 23, No. 2, 2000, pp. 206–214, doi:10.2514/2.4540.

[19] Ainscough, T., Zanetti, R., Christian, J., and Spanos, P. D., "Q-Method Extended Kalman Filter," *AIAA Journal of Guidance, Control, and Dynamics*, Vol. 38, No. 4, 2015, pp. 752–760, doi:10.2514/1.G000118.

[20] Reynolds, R. G., "Asymptotically Optimal Attitude Filtering with Guaranteed Convergence," *Journal of Guidance, Control, and Dynamics*, Vol. 31, No. 1, 2008, pp. 114–122, doi:10.2514/1.30381.

[21] Mueller, M. W., Hehn, M., and D'Andrea, R., "Covariance Correction Step for Kalman Filtering with an Attitude," *Journal of Guidance, Control, and Dynamics*, Vol. 40, No. Special Issue on The Kalman Filter and Its Aerospace Applications, 2017, pp. 2301–2306, doi:10.2514/1.G000848.

[22] Crassidis, J. L. and Markley, F. L., "Unscented Filtering for Spacecraft Attitude Estimation," *AIAA Journal of Guidance, Control, and Dynamics*, Vol. 26, No. 4, 2003, pp. 536–542, doi:10.2514/2.5102.

[23] Cheng, Y. and Crassidis, J. L., "Particle Filtering for Attitude Estimation Using a Minimal Local-Error Representation," *AIAA Journal of Guidance, Control, and Dynamics*, Vol. 33, No. 4, 2010, pp. 1305–1310, doi:10.2514/1.47236.

[24] Bonnabel, S., "Left-Invariant Extended Kalman Filter and Attitude Estimation," *in Proceedings of the 46th IEEE Conference on Decision and Control*, pp. 1027–1032. New Orleans, LA, USA, Dec. 12-14, 2007.

[25] Bonnabel, S., Martin, P., and Salaün, E., "Invariant Extended Kalman Filter: Theory and Application to a Velocity-Aided Attitude Estimation Problem," *in Proceedings of Joint 48th IEEE Conference on Decision and Control and 28th Chinese Control Conference*, pp. 1297–1304. Shanghai, P.R. China, December 16-18, 2009.

[26] Martin, P. and Salaün, E., "Invariant Observers for Attitude and Heading Estimation from Low-Cost Inertial and Magnetic Sensors," *in Proceedings of the 48th IEEE Conference on Decision and Control*,

pp. 1039–1045. New Orleans, LA, USA, Dec. 12-14, 2009.

[27] Bonnabel, S., Martin, P., and Rouchon, P., "Symmetry-Preserving Observers," *IEEE Transactions on Automatic Control*, Vol. 53, No. 11, 2008, pp. 2514–2526, doi:10.1109/TAC.2008.2006929.

[28] Barczyk, M. and Lynch, A. F., "Invariant Observer Design for a Helicopter UAV Aided Inertial Navigation System," *IEEE Transactions on Control Systems Technology*, Vol. 21, No. 3, 2013, pp. 791–806, doi:10.1109/TCST.2012.2195495.

[29] Barrau, A. and Bonnabel, S., "Intrinsic Filtering on Lie Groups with Applications to Attitude Estimation," *IEEE Transactions on Automatic Control*, Vol. 60, No. 2, 2015, pp. 436–449, doi:10.1109/TAC.2014.2342911.

[30] Altmann, S., *Rotations, Quaternions, and Double Groups*, Oxford Science Publication, Clarendon, Oxford, 1986. 1986, pp. 201–223.

[31] Crassidis, J. L. and Junkins, J. L., *Optimal Estimation of Dynamic Systems*, CRC Press, Boca Raton, FL, 2nd ed., 2012. 2012, Chap. 5, pp. 451–462.

[32] Gai, E., Daly, K., Harrison, J., and Lemos, L., "Star-Sensor-Based Satellite Attitude/Attitude Rate Estimator," *Journal of Guidance, Control, and Dynamics*, Vol. 8, No. 5, 1985, pp. 560–565, doi:10.2514/3.56393.

[33] Thébault, E., et al., "International Geomagnetic Reference Field: the 12th Generation," *Earth, Planets and Space*, Vol. 67, No. 79, 2015, pp. 1–19, doi:10.1186/s40623-015-0228-9.